Distinct roles of Nrf1 and Nrf2 in coordinately controlling the anti-ageing response

Da Lyu[a,b,c], Meng Wang[a], Lu Qiu[a,d], Shaofan Hu[a], Yiguo Zhang[b,c,*]

[a] Bioengineering College and Graduate School, Chongqing University, No. 174 Shazheng Street, Shapingba District, Chongqing 400044, China

[b] Chongqing University Jiangjin Hospital, School of Medicine, Chongqing University, No. 725 Jiangzhou Avenue, Dingshan Street, Jiangjin District, Chongqing 402260, China

[c] The Laboratory of Cell Biochemistry and Topogenetic Regulation, College of Bioengineering, Chongqing University, No. 174 Shazheng Street, Shapingba District, Chongqing 400044, China

[d] School of Life Sciences, Zhengzhou University, No. 100 Kexue Avenue, Zhongyuan District, Zhengzhou 450001, Henan, China.

* Correspondence to YZ: yiguozhang@cqu.edu.cn ; Tel.: +86-23-6510-2507

Abstract:

Nuclear factor erythroid-derived 2-like 1 (Nrf1, encoded by *Nfe2l1*), an essential transcription factor of the cap'n'collar basic-region leucine zipper (CNC-bZIP) family, is highly conserved with its homologous Nuclear factor erythroid-derived 2-like 2 (Nrf2, encoded by *Nfe2l2*). Of note, Nrf1 possesses a remarkable anti-senescence potential, but it has not been comprehensively characterized to date. Conversely, *Nrf1α*$^{-/-}$ cells undergoing senescence display hallmarks of senescence, comprising heightened activity of senescence-associated β-galactosidase, decreased cell vitality, cell growth arrest, and increased expression of the senescence-associated secretory phenotype. Further investigation showed cellular senescence in *Nrf1α*$^{-/-}$ cells is not a consequence of Nrf2 accumulation. On the contrary, Nrf2 could alleviate, but not halt or reverse, senescence of *Nrf1α*$^{-/-}$ cells. This is predominantly attributable to the fact that, different from Nrf2, the deficiency of Nrf1 brings about activation of both p21 and RB pathways independently of p53, but disrupts STAG2- and SMC3-dependent chromosomal homeostasis so to drive cell senescence. Here, we discover the significant anti-senescence capacity of Nrf1 and highlight two mechanisms underlying the protective function of Nrf1, which stem from its response to stress and its role in maintaining cellular homeostasis.

Keywords: Nrf1; Nrf2; anti-senescence; p21; STAG2; SMC3; stress response; cellular homeostasis

1. Introduction

Ageing is a continuously changing multifactorial process of decline in physiological function that affects higher organisms. It poses threats to health and increases the risk of disease and mortality [1-3]. Currently, the global ageing phenomenon continues to accelerate [4], leading to a rise in the prevalence of morbiditydue to age-related illnesses (e.g., heart failure, diabetes, atherosclerotic disorders). This trend presents significant challenges in both medical and socio-economic domains [5, 6]. To investigate the potential for increased longevity and devise superior anti-ageing interventions, research on the mechanisms of ageing has highlighted certain markers or pillars of ageing, including genomic instability, progenitor exhaustion/dysfunction, and cellular senescence [7-9]. Among these factors, cell senescence significantly gives rise to ageing process and age-associated disorders. This underscores the potentiality of targeting senescent cells as an effective tactics for extending lifespan and preventing and treating age-related chronic diseases [10-12].

Cell senescence is a response to acute or chronic injuries stemming from intrinsic stress and extrinsic stimuli. Its classical characteristics include irreversible proliferative arrest and a pronounced pro-inflammatory secretory phenotype [7, 13]. Cellular senescence drives organismal aging and promotes age-associated diseases. Research indicates that inducing aging-related phenotypes through senescent cells transplantation, and an increase in mortality through senescent cells spread in host tissues [14]. Conversely, the extermination of senescent cells mitigates the progression of age-associated phenotypes in vivo [15]. The focal aggregation of senescent cells in non-proliferative disorders contributes to the senescence-associated secretory phenotype (SASP) that accounts for the pathogenesis of these diseases [16, 17]. In preclinical models, interventions targeting senescent cells have demonstrated alleviation or prevention of numerous diseases [14, 18]. Thus, targeting cellular senescence has emerged as a novel strategy for anti-ageing and extending healthspan.

Nuclear factor erythroid-derived 2-like 1 (Nrf1), identified as early as 1990s, is a transcription factor that is highly conserved and present in various animal tissue cells and pertains to the cap'n'collar-basic-region leucine zipper (CNC-bZIP) family [19]. By forming heterodimers with other bZIP proteins, Nrf1 regulates stress-responsive genes [20, 21]. The primary target genes of Nrf1 extensively participate in various biological processes, including oxidative stress, mitochondrial quality control, proteasome regulation, glucose metabolism, and genetic homeostasis [21-25]. Primary and secondary senescence are profoundly linked to imbalances in these biological functions [26, 27]. Accumulating evidence has revealed that impaired Nrf1 function can trigger the

occurrence and progression of numerous aging-related pathologies (e.g., atherosclerosis, Parkinson's disease). Thus, the potential function of Nrf1 in anti-senescence remains unexplored [21-25]. Therefore, it is necessary to examine the role of Nrf1 and its regulatory manners during cellular senescence.

In this research, we evaluated the senescence features of *Nrf1α*$^{-/-}$ cells (stable Nrf1 knockout HepG2 and LO2 cell lines) within two distinct established senescence models. Our aim was to elucidate the anti-senescence role and function of Nrf1. Further, we discovered that the anti-senescence function of Nrf1 is independent of Nuclear factor erythroid-derived 2-like 2 (Nrf2). Nrf2 activation, triggered by the absence of autophagy in *Nrf1α*$^{-/-}$ cells, represents a limited compensation mechanism against anti-senescence functions following Nrf1 deficiency in cells. However, Nrf2 cannot fully substitute for Nrf1. This largely stems from the fact that Nrf1 possesses distinct characteristics compared to Nrf2, specifically its unique dual anti-senescence attributes involving stress responsiveness and homeostatic maintenance. Nrf1 exhibits p53-independent characteristics in the stress response and Stromal antigen 2 (STAG2)/Structural maintenance of chromosomes 3 (SMC3)-dependent characteristics in homeostasis maintenance. These findings enhance our comprehension of the physiological and pathological functions of Nrf1 in biological systems. They also offer a theoretical foundation for the formulation of tactics designed to decelerate the process of ageing and mitigating age-associated disorders, with the Nrf1 pathway as a reference point.

2 Experimental section

2.1 Cell culture and chemical solvents

HepG2 cells were sourced from American Type Culture Collection, LO2 cells were sourced from the National Infrastructure for Cell Line Resource. Additionally, short tandem repeat(STR) typing maps and authentication profiles were employed to confirm the fidelity of both cell lines (performed by Shanghai Biowing Applied Biotechnology Co., Ltd., Shanghai, China). *Nrf1α*$^{-/-}$ and *Nrf2*$^{-/-}$cells were previously generated by Qiu et al using wild-type (WT) HepG2 and LO2 cells in our laboratory, and were subsequently identified in this study. (Fig. S1). All experimental cells were nourished using basic DMEM (Gibco, Grand Island, NY, USA) supplemented with 10% FBS (Gibco) and 1% antibiotics (penicillin–streptomycin, Gibco). The cells were incubated at 37∟ with 5% CO_2. Relevant resources including equipments, reagents, software tools used in this work are presented in Supplementary Table 1.

2.2. MTT assay

To analyze the viability of the experimental cells, the MTT assay was performed. Cells were incubated overnight in cell culture plates (96-well, flat bottom) at a plating concentration of 1∟×∟10^2∟cells/uL. The experimental cells were appropriately manipulated according to experimental requirements, at the end of treatment, the selected wells were appended with MTT (5 mg/mL, Molekula, Darlington, UK) , placed in an incubator and maintained at 37 degrees Celsius for a duration of 4 hours. Subsequently, the solution within the orifice was removed, and dimethyl sulfoxide (Solarbio) was dispensed to solubilize the reaction product. Absorbance readings were taken at a wavelength of 490∟nm.

2.3 Senescence-associated beta-galactosidase (SA-β-gal) staining assay and activity assay

An SA-β-gal staining kit (CST, Danvers, MA, USA) was employed to assess cellular senescence following specific protocol described by the company. The experimental cells were appropriately manipulated according to experimental requirements. Following treatment, cells underwent two PBS washes and were fixed in a formulated fixative for 15 min at ambient temperature. Subsequently, the cells underwent three 5-min PBS washes and were incubated with a staining solution at 37∟ without CO2 overnight.

The cells were examined and imaged using a microscope. Blue-stained cells, indicating β-gal positivity, were quantified.

Cytosolic SA-β-gal levels were measured by β-gal activity assay kit (Solarbio). Samples and standard solutions were prepared, sonicated, and processed according to the provided instructions, and the optical density (OD) was determined at a wavelength of 400 nm. The BCA methodology was employed to quantify total extracted proteins, employing a protein assay reagent kit (ApplyGen, Beijing, China). β-gal activity was determined and calculated following specific protocol described by the company.

2.4 Cell senescence models

Two distinct models of senescence were established: a natural senescence model (chronological aging) and a D-galactose (D-gal)-induced senescence model. Experimental cells (LO2 and HepG2 cells) were plated into cell culture plates (96-well, flat bottom) and incubated until reaching 80% confluence. Subsequently, culture medium was refreshed. For establishing the natural senescence model , the cells were continuously cultivated for varying durations (24, 48, or 72 h). Cell senescence was assessed via SA-β-gal staining, while cell survial and apoptosis was analyzed through an MTT assay. The establishment of the natural senescence model was guided by the outcomes of these assessments. For establishing the D-gal-induced senescence model, briefly, various concentrations of D-gal (1, 5, 10, 20, 30, 40, and 50 mg/ml) were introduced into the medium and maintained for varying durations (24, 48, or 72 h) to induce cellular senescence. The optimal concentration and time point for D-gal induction were determined through the SA-β-gal assay and the MTT method.

2.5 Cell proliferation and colony formation assay

The experimental cells were plated into cell culture plates (96-well, flat bottom), and were appropriately manipulated according to experimental requirements. Following treatment, the selected wells were appended with Cell Counting Kit-8 (CCK-8) (10 μL, Solarbio) and placed in an 5% CO_2 incubator and maintained at 37 degrees Celsius for a duration of 2 hours. OD were recorded for each well at 450 nm to calculate cell proliferation.

In the colony formation experiments, cells were cultured in complete media at 500 cells per well using cell culture plates (6-well, flat bottom) for 24 h. The experimental cells were then subjected to various treatments, depending on the specific experiment, for 10–14 days. The culture media were replaced every third day. Subsequently, the cell colonies were stabilized using 4% paraformaldehyde (Sangon, Shanghai, China) , then crystal violet stain reagent (1%; Solarbio) was used to stain colonies at ambient temperature for 20 min , followed by two rinses with PBS. Finally, colonies were photographed and counted.

2.6 Cell cycle assay

Initially, cells were pelleted through centrifugation, followed by rinsing with cold PBS and a subsequent centrifugation step. They were then fixed with pre-cooled 75% ethanol overnight. Prior to analysis, the cells underwent three PBS washes. Subsequently, they were resuspended in a staining solution (Yeasen, Shanghai, China), followed by incubation in the dark for at least 30 min at ambient temperature. The cell cycle was meticulously evaluated utilizing a flow cytometer (Beckman Coulter, Brea, CA, USA). FlowJo V10 software (BD Biosciences) was utilized to perform data analysis.

2.7 Real-time quantitative PCR (qRT-PCR) analysis

RNA isolation was accomplished utilizing an RNA extraction kit (Promega, Madison, WI, USA). The production of cDNA was performed through reverse transcription utilising the cDNA Synthesis Kit (Yeasen) following specific protocol described by the company. Quantification of relative mRNA levels was assessed using the CFX Connect real-time PCR system (Bio-Rad, Hercules, CA, USA). The reaction system qPCR Master Mix (GoTaq®, Promega) was utilized with the following specific protocol described by the company. All reactions were conducted in triplicate in a multiplate plate(96-well, Bio-Rad), and melting curve analysis was employed to determine specific amplification. Relative mRNA levels were standardized to those of the control gene β-actin, utilizing the $2^{-\Delta\Delta CT}$ method. Sequence information of Primers for qRT-PCR is summarized in Supplementary Table 1.

2.8 Western blot analysis

The experimental cells underwent two PBS washes and were lysed using a lysis buffer (Yeasen), Total proteins were extracted and this extraction was performed at 4℃. A BCA protein quantification kit (Yeasen) was performed to ascertain concentration. The protein samples were subsequently separated utilizing SDS-polyacrylamide gel electrophoresis (PAGE) on polyacrylamide gels (concentration range: 8 – 15%), following this, the samples were then transferred onto a polyvinylidene fluoride membranes (Thermo) utilizing a wet transfer manner. Subsequently, Membranes were placed in the incubation box and blocked with fast blocking buffer(Yeasen). Appropriate primary antibodies were incubated overnight at a controlled temperature of 4℃, followed by appropriate secondary antibodies (horseradish peroxidase-conjugated; Sangon) were incubated. After 2 h incubation at ambient temperature, protein bands were identified with an chemiluminescent western blot detection kit (Yeasen). Finally, quantification was performed utilizing iBright Analysis software (Thermo). β-actin was employed as an internal standard. Details of the antibodies utilized are available in Supplementary Table 1.

2.9 Small interfering RNA (siRNA) transfection

Tsingke (Beijing, China) provided siRNAs specifically targeting human Nrf2, STAG2, and SMC3 and a scrambled control siRNA. The experimental cells were transfected utilising Lipofectamine™ 3000 (Thermo) following specific protocol described by the company. Post-transfection, cells were permitted to grow for 24 h, after which they were subjected to the indicated treatments for further experimentation. The specific sequences of the SiRNA oligonucleotide are detailed in Supplementary Table 1.

2.10 Bioinformatics analysis

The total RNAs from each cell line (LO2 and *Nrf1*$^{-/-}$ LO2 cells) were isolated and purified with an RNA extraction kit (Promega) and subsequently all samples were sequenced at the Beijing Genomics Institute (Shenzhen, China). RNA sequencing data for other cell lines (WT HepG2 and HEK293 cells, *Nrf1*$^{-/-}$ HepG2 cells, and Nrf1 HEK293 cells) were acquired from prior studies conducted within our research facility [28, 29]. Evaluate all reads for filtering, Subsequently, they were aligned to the Refseq Human Genome GRCh38.p12 utilising Bowtie2 [30] and HISAT software [31]. Gene expression values were determined using RNA-Seq by Expectation-Maximization (RSEM) [32]. Significantly differentially expressed genes (DEGs), exhibiting a false discovery rate <0.001 and log2 fold change >1 or <-1 , were identified. The DAVID tool was employed to perform Gene Ontology annotation enrichment analysis of the DEGs. A protein-protein interaction (PPI) network

of the DEGs was generated utilizing the STRING database. Key nodes (hub genes) in the PPI network were identified using the Cyotoscape plugin cytoHubba and MCODE [33, 34]. Significant hub genes were identified through cross-comparison between datasets and validated via qRT-PCR.

2.11 Luciferase reporter assay

The antioxidant response element (ARE) and its mutant forms of indicated gene were subcloned into a PGL3-promoter vector to produce reporter plasmids. The ARE-Luc reporter constructs or mutant ARE-Luc reporter constructs were co-transfected into HepG2 cells along with either an Nrf1 expression construct or vector control (empty pcDNA3.1 vector). The pRL-TK plasmid, coding for Renilla luciferase, served as the transfection control in all transfections. Luciferase assays were conducted post-transfection for 24 h utilizing a dual-reporter assay kit (Promega) following the company protocol. Firefly luciferase values were standardized to Renilla luciferase signals.

2.12 Chromatin immunoprecipitation (ChIP)-sequencing analysis

The date for ChIP-sequencing were acquired from the ENCODE ChIP-Seq repository (https://www.encodeproject.org). The project identifier for the ENCODE study is ENCSR543SBE (Nrf1 in Homo sapiens HepG2 cells).

2.13 Statistical analysis

Experimental data is displayed in the form of the average value plus or minus the standard deviation. The statistical analysis of data was conducted utilising Student's t-test, Mann-Whitney test or two-way ANOVA with SPSS 22.0 software (IBM, Armonk, NY, USA). A statistically significant disparity was considered at probability (P) values < 0.05.

3 Results

3.1 *Nrf1α*$^{-/-}$ cells acquire typical features of senescent cells

To accurately evaluate Nrf1's role in cellular senescence, we established two distinct senescence cell models: a natural senescence model and a D-gal-induced senescence model. The natural senescence model was established by subjecting cells to 48 h of continuous cultivation with complete media. The D-gal-induced senescence model was established by subjecting cells to D-gal treatment (20 mg/mL) for 48 h. This was based on an integrated assessment of SA-β-gal staining and MTT assay outcomes, which revealed a high degree of senescence accompanied by a moderate degree of apoptosis (Fig. S2). In both senescence models, *Nrf1α*$^{-/-}$ cells exhibited enlarged and flattened senescent cell morphologies compared to WT cells (Fig. 1A, 1B). Subsequently, we performed SA-β-gal staining to assess β-gal activity in WT and *Nrf1α*$^{-/-}$ cells. As shown in Fig. 1C and 1D, *Nrf1α*$^{-/-}$ cells displayed a notably higher SA-β-gal-positivity compared to WT cells. Consistent with these findings, the activity of enzymes in *Nrf1α*$^{-/-}$ cells was markedly increased in comparison with that in WT cells (Fig. 1E, 1F). Senescent cells characteristically exhibit impaired proliferation. Therefore, we proceeded to compare the proliferative capacity of WT and *Nrf1α*$^{-/-}$ cells in our senescence cell models. Compared to WT cells, *Nrf1α*$^{-/-}$ cells exhibited a lower number of colonies in the colony formation assay (Fig. 1G, H, left) and a greater reduction in cell proliferation rate, as assessed via the CCK-8 colorimetric method (Fig. 1G, H, right). Another crucial trait of senescent cells is their irreversible arrest in the cell cycle. Therefore, we analyzed the distribution of WT and *Nrf1α*$^{-/-}$ cells in different cell cycle phases through flow cytometry (Fig. S3). The results suggested that Nrf1-deletion led to a marked elevation in the G1 cell population, whereas the proportions of S and G2/M cells decreased significantly in our senescence cell models (Fig. 2H). These findings indicate that

Nrf1α$^{-/-}$ cells experience cell cycle arrest in the G1 phase.

.

3.2 Nrf1-deletion induces SASP and the accumulation or reduction of senescence biomarkers through the p21 and Retinoblastoma (RB) signal transduction pathway

Senescent cells acquire autocrine/paracrine abilities, producing a plethora of proinflammatory cytokines, proteases, and other molecules, collectively referred to as the SASP. The SASP factors play pivotal roles in secondary senescence, driving self-senescence via an autocrine feedforward loop and inducing dysfunction and growth arrest in neighboring cells [35]. In WT and *Nrf1α*$^{-/-}$ cells in our senescence cell models, we analyzed the relative expression of canonical SASP genes that are frequently upregulated in other senescent cells using qPCR method. As illustrated in Fig. 2A–G, compared to those in WT cells (control), mRNA levels of *IL-1α, IL-1β, IL-6, IL-8, CXCL-3, CXCL-10*, and *MMP1* were significantly increased in *Nrf1α*$^{-/-}$ cells. Ki67 and LaminA are frequently employed as negative molecule markers of senescent cells. Thus, we estimated the expression of Ki67 and LaminA proteins in both WT and *Nrf1α*$^{-/-}$ cells in our senescence cell models. In contrast to those in WT cells, the levels of Ki67 and LaminA proteins were notably decreased in *Nrf1α*$^{-/-}$ cells, as revealed by western blotting method (Fig. 2I, i1 and i2). These results align with prior results demonstrating G1 phase arrest in *Nrf1α*$^{-/-}$ cells.

Indeed, senescence is a progressive transition from an early (pre-senescent) to a complete (full senescence) state, accompanied by chromatin remodeling and SASP production. The pivotal point in this process occurs when cells shift from a transient state to a stable cell cycle arrest [36]. Hence, to evaluate the signal transduction pathway involved in senescence induction by Nrf1-knockout (Nrf1-KO), we performed western blotting method and assessed several specific cell cycle regulatory proteins in our senescence cell models. A notable elevation in the levels of p21 protein was observed in *Nrf1α*$^{-/-}$ cells compared to WT cells (Fig. 2I, i4). Additionally, the levels of CDK2 and cyclin D1 proteins, which are the principal modulators of the G1/S checkpoint in the cell cycle, were reduced in *Nrf1α*$^{-/-}$ cells (Fig. 2I, i5 and i6). Consequently, this led to a decrease in the activation of RB kinase, resulting in significant inhibition of RB phosphorylation (pRB) (Fig. 2I, i7) and a subsequent reduction in E2F1 protein levels in *Nrf1α*$^{-/-}$ cells (Fig. 2I, i8), ultimately leading to cell cycle arrest. These results indicate that Nrf1-KO induces cell senescence by suppressing RB phosphorylation via the p21 and RB signal transduction pathways.

3.3 Dysfunctional autophagy in *Nrf1α*$^{-/-}$ cells contributes to cell senescence

Insufficient autophagy is a well-documented mechanism of induced cell senescence [37]. To validate the suppression of autophagy in *Nrf1α*$^{-/-}$ cells, we examined autophagy-associated marker molecules in WT and *Nrf1α*$^{-/-}$ cells in our senescence cell models using the qPCR method. As illustrated in Fig. 3A–G, the mRNA expression levels of *ULK1*, *Beclin1, ATG4A, ATG7, ATG9A, ATG10,* and *ATG12* were markedly decreased in *Nrf1α*$^{-/-}$ cells in comparison to the control. We further investigated the protein expression of autophagy-associated markers using the western blotting method, and similar results were observed. The concentrations of ULK1, Beclin1, ATG5, ATG7, ATG9A, ATG10, and ATG13 proteins were remarkable reduced, while the concentrations of LC3-II protein and the autophagic substrate p62 were markedly enhanced in *Nrf1α*$^{-/-}$ cells in comparison with the control (Fig. 3H). To corroborate the impact of autophagy blockade in *Nrf1α*$^{-/-}$ cells, we also examined autophagic flux, which defines changes in the amount of autophagic activity and provides a more accurate assessment of autophagic activity. Subsequently, we employed rapamycin (Rapa,

an mTOR inhibitor) and chloroquine (CQ, an autophagy inhibitor) to stimulate or inhibit autophagy in both WT and *Nrf1α*$^{-/-}$ cells in our senescence cell models. Following Rapa or CQ treatment, autophagy markers were assessed through qPCR and western blotting. As expected, mRNA expression of *ULK1, Beclin1, ATG4A, ATG7, ATG9A, ATG10,* and *ATG12* and proteins expression of ULK1, Beclin1, ATG5, ATG7, ATG9A, ATG10, and ATG13 were significantly decreased, and LC3-II and p62 levels were markedly enhanced in *Nrf1α*$^{-/-}$ cells in comparison with the control after treatment with Rapa (Fig. S4) or CQ (Fig. S5). These results suggest that Nrf1 deletion inhibits autophagic flux. In summary, Nrf1-KO leads to decreased autophagic activity via impaired expression of autophagic markers, subsequently accelerating cell senescence.

3.4 Accumulation of Nrf2 exerts a compensatory anti-senescence effect in response to Nrf1 deficiency

The aforementioned findings indicate that the accumulation of p62 is a result of impaired autophagic activity in *Nrf1α*$^{-/-}$ senescent cells, potentially result in the activation of the p62-Keap1-Nrf2 axis(Fig. 4A). Therefore, we sought to investigate whether autophagy reduction and p62 accumulation in *Nrf1α*$^{-/-}$ senescent cells could activate this axis in our cellular senescence models. As shown in Fig. 4B, western blotting revealed a notable elevation in p62 levels, accompanied by a reduction in the level of Keap1 protein (An inhibitor of Nrf2) in *Nrf1α*$^{-/-}$ cells, ultimately resulting in Nrf2 accumulation compared to the control (WT cells). Additionally, we evaluated the mRNA levels of Nrf2 via qPCR and found no considerable change in Nrf2 expression in *Nrf1α*$^{-/-}$ cells as opposed to the control (Fig. 4C). Collectively, these findings demonstrate that the suppression of autophagy leads to an excess buildup of p62, which in turn impedes the binding of Keap1 to Nrf2, ultimately triggering Nrf2 accumulation in *Nrf1α*$^{-/-}$ cells. We aimed to clarify the capacity of Nrf2 in Nrf1 deletion-induced cellular senescence. Nrf2 was specifically silenced using siRNA in *Nrf1α*$^{-/-}$ HepG2 cells, resulting in the inhibition of Nrf2 protein expression in comparison to the control (Fig. 4D). The mRNA expression of crucial SASP factors, namely *IL-1α, IL-1β, IL-6, IL-8, CXCL-3, CXCL-10*, and *MMP1*, were remarkable enhanced in *Nrf1α*$^{-/-}$ HepG2 cells with Nrf2 silencing, as compared to control cells in our senescence models (Fig. 4E–K). Additionally, the proein expression of Ki67 was substantially decreased in Nrf2 siRNA-transfected cells relative to the control cells (Fig. 4L, l1). Meanwhile, Nrf2 knockdown significantly enhanced the levels of p53 and p21 proteins (Fig. 4L, l2 and l3) while concomitantly reducing the expression of CDK2, cyclin D1, pRB, and E2F1 proteins (Fig. 4L, l4–l7). These results indicated that *Nrf1α*$^{-/-}$ HepG2 cells underwent accelerated senescence when treated with siNrf2, exhibiting typical features of senescent cells, such as an upregulation of SASP expression, degradation of the proliferation marker Ki67, and activation of the p21-RB axis. This indicates that the atypical accumulation of Nrf2 protein in *Nrf1α*$^{-/-}$ cells significantly delays senescence. To confirm the capacity of Nrf2 in cell senescence, we assessed senescence through staining (Fig. 5A) and quantitative measurement of SA-β-gal activity (Fig. 5B) within both WT and *Nrf2*$^{-/-}$ HepG2 cells in our cellular senescence models. The results suggested that Nrf2-KO significantly increased enzyme activity. We observed that *Nrf2*$^{-/-}$ cells exhibited fewer colonies compared to WT cells, as measured by the colony formation assay in our cellular senescence models (Fig. 5J, left). Additionally, the CCK-8 assay showed a decrease in cell proliferative capacity upon Nrf2-KO (Fig. 5J, right). We analyzed the impact of Nrf2-KO on the cell cycle via flow cytometry in our cellular senescence models and found a marked increase in the G1 cell population and a marked decrease in the S phase in *Nrf2*$^{-/-}$ cells in comparison to WT cells (Fig. 5K–L), indicating that Nrf2-KO induces G0/G1 phase cell cycle arrest. Furthermore, a notable elevation in the mRNA levels of *IL-1α, IL-1β, IL-6, IL-8, CXCL-3, CXCL-10,* and *MMP1* in *Nrf2*$^{-/-}$ cells was observed in our cellular senescence models. Nrf2-KO conspicuously promoted the secretion of SASP factors (Fig. 5C–I). In addition, to assess senescence induction, we evaluated characteristic markers of senescence in our senescence cell models using the western blotting method. *Nrf2*$^{-/-}$ cells exhibited a pronounced decrease in Ki67 and LaminA proteins. These results definitely

indicated that *Nrf2*$^{-/-}$ cells had attained the senescent state. Based on the aforementioned results, We inferred that Nrf2 exerts a crucial contribution to anti-senescence activity. Upon Nrf1-KO, activated Nrf2 accumulates, markedly delaying senescence in Nrf1-deficient cells. This demonstrates the essential compensatory overexpression of Nrf2 in defense against cell senescence in response to Nrf1 deletion.

3.5 Anti-senescence effects of Nrf1 and Nrf2 are mediated through the suppression of the p21-RB axis, with a greater contribution from Nrf1 compared to Nrf2

Our prior results suggest that the activation of Nrf2 delays Nrf1-KO-induced cell senescence, but it cannot halt or reverse this process. This raises the question of why Nrf2 is unable to completely compensate for the the deficiency of Nrf1. In order to address this query, we employed the western blotting method and analyzed the expression of well-established markers associated with the p21 and RB signaling pathway in both WT and *Nrf2*$^{-/-}$ cells. As shown in Fig. 5M, Nrf2-KO increased the levels of p53 and p21 proteins. In accordance with these results, we noted a marked diminution in the expression of CDK2, cyclin D1, pRB, and E2F1 proteins in *Nrf2*$^{-/-}$ cells in comparison to WT cells (Fig. 5M, m5–m8). These findings are consistent with our earlier observations of the levels of these markers in *Nrf1α*$^{-/-}$ cells transfected with siNrf2 (Fig. 4L, l2–l7). Previously, we conducted the same experiment and analyzed the levels of p53, p21, CDK2, cyclin D1, pRB, and E2F1 proteins in *Nrf1α*$^{-/-}$ cells. An elevation of p21 and a reduction of p53, CDK2, cyclin D1, pRB, and E2F1 were observed in *Nrf1α*$^{-/-}$ cells compared to WT cells (Fig. 2I, i3–i8). Taken together, these findings validate the inhibition of the p21-RB axis by Nrf1 is independent of p53, unlike Nrf2, which is dependent on p53. Furthermore, this demonstrates the superior regulatory potency of Nrf1 in modulating the p21-RB axis compared with Nrf2.

3.6 Nrf1, not Nrf2, depends on STAG2 and SMC3 to sustain cellular homeostasis for anti-senescence

While both Nrf1 and Nrf2 pertain to the same family, distinct from Nrf2, Nrf1 is an essential regulator of cellular homeostasis. This suggests that we can comprehend its anti-senescence function by examining Nrf1's critical role in maintaining homeostatic equilibrium, thereby elucidating the disparities between Nrf1 and Nrf2 in anti-senescence.

Through transcriptome sequencing analysis, we identified critical genes that are differentially expressed and are under the regulation of Nrf1, which maintain cellular homeostasis and prevent senescence. After normalizing the gene expression datasets, screening and conducting functional enrichment analysis of DEGs, we identified 18 candidate crucial genes through a PPI network and module analysis (Fig. 6A). Subsequently, we conducted further core analysis and, following qPCR validation, narrowed down our focus to two core targets, namely, STAG2 and SMC3, which are primarily associated with cellular homeostasis (Fig. 6B and S6). STAG2 and SMC3, as components of the cohesin complex, participate in preserving chromosomal number and structure integrity, ensuring chromosomal stability, and thereby contributing to overall cellular homeostasis. It is well-established that STAG2 and SMC3 are essential for cell viability. To explore the function of STAG2 (or SMC3) in cell senescence in our senescence cell models, we employed specific siRNAs to silence their expression in WT HepG2 cells. We then assessed cell senescence markers (Fig. 7). Senescence was assessed quantitatively through SA-β-gal activity (Fig. 7A) in both WT HepG2 cells and STAG2 (or SMC3)-silenced HepG2 cells. The results suggested a significant increase in enzyme activity in our senescence cell models upon STAG2 (or SMC3) knockdown. The mRNA levels of classical SASP factors, *IL-1α, IL-1β, IL-6, IL-8, CXCL-3, CXCL-10*, and *MMP1* were significantly increased in STAG2 (or SMC3)-silenced cells in our senescence cell models (Fig. 7B–H). Senescence biomarker molecules Ki67 and LaminA exhibited a sharp decline in protein levels in STAG2 (or SMC3)-silenced cells in our senescence cell models (Fig. 7I, i1–i3). Notably, the protein expression of p53 and p21 showed remarkable enhancement (Fig. 7I, i4 and i5), while the

expression of CDK2, cyclin D1, pRB, and E2F1 proteins were dramatically downregulated in STAG2 (or SMC3)-silenced cells compared with the controls in our senescence cell models (Fig. 7I, i6–i9). These results demonstrated the essential role of STAG2 (or SMC3) in cell senescence and the inducement of senescence upon STAG2 (or SMC3) silencing in our senescence cell models.

To further clarify whether STAG2 and SMC3 are involved in senescence induced by Nrf1-KO, we evaluated their expression in both WT and *Nrf1α*$^{-/-}$ cells in our senescence cell models. As indicated in Fig. 6C and 6D, a dramatically downregulation in the levels of STAG2 and SMC3 mRNA in *Nrf1α*$^{-/-}$ cells was observed. Similar outcomes are depicted in Fig. 6G, which demonstrated a notable reduction in the levels of STAG2 and SMC3 proteins in *Nrf1α*$^{-/-}$ cells (Fig. 6G, g1 and g2). These results underscore that Nrf1-deletion results in the inhibition of STAG2 and SMC3 in *Nrf1α*$^{-/-}$ cells and induces significant cell senescence. Furthermore, we investigated whether Nrf2 can regulate the expression of STAG2 and SMC3 as Nrf1. As shown in Fig. 6E, 6F, and 6G (g4 and g5), No substantial changes were observed in the levels of STAG2 and SMC3 mRNA and protein expression when Nrf2 was silenced through siRNA compared to the vector control in our senescence cell models. The same observations were made for Nrf2-KO cells compared to WT cells in our senescence cell models. These results validated that Nrf2 does not affect the expression of STAG2 and SMC3. We then explored whether Nrf1 directly regulates STAG2 and SMC3 expression through binding to Nrf1-binding motifs within their promoter regions. We analyzed the proximal promoters of these genes for potential AREs, which are typical Nrf1-binding elements. We found three conserved ARE promoter elements in *STAG2* and *SMC3* for Nrf1 binding. We then conducted luciferase reporter assays and observed markedly enhanced luciferase activity upon transfection with STAG2/SMC3-ARE2-plasmid constructs compared to the control group. This activation was abolished when mutated ARE plasmid was transfected (Fig. 6I). Investigation of the Encode database revealed Nrf1 ChIP-sequencing data from HepG2 cells, which elucidated notable enrichment signals in STAG2 and SMC3 promoter regions (Fig. 6H). These results together suggest that, unlike Nrf2, Nrf1 mediates the activation of STAG2 and SMC3 expression by specifically interacting with the AREs located in the promoter regions of the *STAG2* and *SMC3* genes, promoting anti-senescence functions.

4 Discussion

Nrf1α$^{-/-}$ cells were evaluated across various senescence models, revealing prominent cellular senescence characteristics at the cellular, molecular, and functional levels. These characteristics encompassed diminished cell vitality, cell cycle cessation, enhanced SA-β-gal expression, increased SASP, elevated or reducted expression of senescence biomarkers (e.g., p21), impaired autophagy, etc. We discovered that the abnormal accumulation of Nrf2 in *Nrf1α*$^{-/-}$ cells does not induces senescence but provides limited alleviation from cellular senescence. *Nrf1α*$^{-/-}$ cell senescence primarily results from the activation of the p53-independent P21-RB axis and the disruption of cellular homeostasis, represented by STAG2- and SMC3-dependent chromosomal homeostasis.

Our study employed two distinct senescence models: a natural senescence model (chronological senescence) and a D-gal-induced senescence model. The natural senescence model, which simulates intrinsic chronological senescence, non-pharmaceutical interventions, reflects a more authentic senescence state [38]. The D-gal-induced senescence model, a widely utilized classic model for drug intervention, is known for its user-friendly approach, minimal adverse effects, and superior survival rates throughout the experimental period [39]. The combined utilization of these two models facilitated a comprehensive exploration of the involvement of Nrf1 in the process of anti-senescence.

Cell senescence, initially described by Hayflick and Moorhead at the cellular level as limited replicative capacity of primary human fibroblasts and termed the “Hayflick limit” [40], is a permanent and irreversible growth arrest.

This phenomenon is characterized by the cessation of cell division, cell cycle arrest, and diminished activity, collectively representing the most prominent hallmarks of senescent cells. Our study demonstrated a G1 phase cell-cycle arrest in *Nrf1α*$^{-/-}$ cells that experienced ceased proliferation and a significant decline in vitality. An elevation in theSA-β-gal activity is considered a representative standard. As expected, *Nrf1α*$^{-/-}$ cells exhibited enhanced SA-β-gal activity.

Senescent cells are identified by their secretion of SASP. The SASP is highly heterogeneous and can induce secondary or paracrine senescence. It typically exerts concurrent and partially conflicting effects on the microenvironment, ultimately culminating in chronic inflammation and progressive fibrosis in numerous pathological conditions [16, 17]. Based on prior research, Nrf1 is considered an inflammation-responsive transcriptional repressor, primarily owing to the following reasons: Nrf1's target genes encompass inflammatory suppressors [41], and Nrf1 maintains multiple aspects of cellular homeostasis, including proteostasis [25]. Our study indicated increased mRNA expression of SASP factors in *Nrf1α*$^{-/-}$ cells. These SASP factors not only enhance their own senescence through autocrine mechanisms but also induce senescence in neighboring cells via paracrine effects. The buildup of decrepit cells and the prolonged impact of SASP on the internal microenvironment within organisms culminate in chronic inflammation.

Quality control becomes dysregulated in senescent cells, underscoring the pivotal role of cell autophagy in cellular senescence [42, 43]. Macroautophagy (hereafter referred to as autophagy) serves as the sole intracellular mechanism for eliminating excess abnormal protein aggregates and damaged organelles. In addition to maintaining protein homeostasis, autophagy performs diverse functions such as pathogen defense, stress response, and cell reprogramming, thereby playing essential roles in cellular and organismal fitness [44]. Accumulating evidence suggests that autophagy suppression can initiate or expedite senescence, while its activation can delay senescence [45]. Therefore, dysregulation of autophagy has emerged as a hallmark and defining criterion of cellular senescence. Our findings suggest that Nrf1 regulates pivotal molecules at various stages of autophagy. We observed a pronounced reduction in autophagy in *Nrf1α*$^{-/-}$ cells, which was validated through autophagic flux measurements, thereby affirming the senescence of *Nrf1α*$^{-/-}$ cells. Notably, we discovered that the lack of autophagy in *Nrf1α*$^{-/-}$ cells results in heightened Nrf2 expression. Prior research has indicated that the levels of Nrf2 mRNA remain largely unchanged in *Nrf1α*$^{-/-}$ cells. However, in our study, a notable elevation in the expression of Nrf2 protein was observed in *Nrf1α*$^{-/-}$ cells in both senescence models. The key observation was that Nrf2 activation results from a lack of autophagy in *Nrf1α*$^{-/-}$ cells. Inhibition of autophagy in *Nrf1α*$^{-/-}$ cells results in significant p62 aggregation. The P62-Keap1 interacting region (KIR) binds to Keap1 in a binding pattern that closely resembles the interaction between Nrf2-ETGE and Keap1. When p62 accumulates, Keap1 becomes sequestered into aggregates, and, in turn, p62 prevents Keap1-dependent degradation of Nrf2. Activation of Nrf2 signaling, also known as p62-dependent Nrf2 activation (a noncanonical pathway). Additionally, in the Keap1-Nrf2-p62 pathway, Nrf2 induces p62 expression, thereby activating Nrf2 through a positive feedback loop.

Nrf1 and Nrf2, initially identified as NF-E2-associated transcriptional regulators, exhibit CNC domains and a bZIP motif and belong to the CNC-bZIP family. They jointly participate in numerous physiological functions, such as oxidative stress, organelle stress (e.g., endoplasmic reticulum stress), maintenance of protein homeostasis, maintenance of glucose and lipid metabolic equilibrium, and cell fate progression, encompassing growth, development, apoptosis, and cancer. However, their mechanisms and effects display diversity, and the regulatory processes involve intricate interactive dialogues [46]. In our study, the activation of Nrf2 in *Nrf1α*$^{-/-}$ cells indicated that Nrf2 exerts a distinct function in the development of senescence in *Nrf1α*$^{-/-}$ cells. *Nrf1α*$^{-/-}$ cells underwent accelerated senescence due to Nrf2-silencing, while *Nrf2*$^{-/-}$ cells exhibited the classic hallmarks of cellular senescence in our senescence cell models. Therefore, the anti-senescence role of

the Nrf2 factor can be reliably identified. Nrf2 activation is not a driver for senescence in *Nrf1α*$^{-/-}$ cells but rather exerts a compensatory anti-senescence effect due to Nrf1 deficiency. Despite the substantial activation of Nrf2, Nrf2 alone is insufficient to replace Nrf1. It only delays senescence in *Nrf1α*$^{-/-}$ cells but does not fully abrogate it.

Senescent cells are arrested at specific cell-cycle phases (e.g., G1, G2). The p53-p21 and p16-RB pathways exert substantial control over cell cycle arrest [47]. Simultaneously, these pathways are responsive to DNA damage and diverse triggering factors, ultimately converging on the regulation of the senescent cell cycle via RB. Activation of RB leads to chromatin modifications that result in the suppression of growth promoters, including E2F. Consequently, RB-induced senescence is irreversible [48]. Our experimental findings indicated the activation of both the p21 and RB signaling pathways in *Nrf1α*$^{-/-}$ cells and *Nrf2*$^{-/-}$ cells, thereby inducing cellular senescence. Moreover, when Nrf2 was knocked down in *Nrf1α*$^{-/-}$ cells, the p21 and RB pathways were further activated, accelerating cellular senescence. Anti-senescence effects of Nrf1 and Nrf2 are mediated through the suppression of the p21 and RB pathways, with a greater contribution from Nrf1 compared to Nrf2. Notably, in contrast to *Nrf2*$^{-/-}$ cells, which exhibited elevated levels of p53 expression, *Nrf1α*$^{-/-}$ cells typically exhibit downregulated p53, with p53 becoming more activated following the shortage of Nrf2 in *Nrf1α*$^{-/-}$ cells. In contrast to Nrf2, Nrf1 exhibited p53-independent anti-senescence activity.

Nrf1 exerts a pivotal effect in maintaining cellular homeostasis. Cellular senescence in *Nrf1α*$^{-/-}$ cells could be attributed to a disruption in cell homeostasis due to Nrf1 deficiency. Our study identified STAG2 and SMC3 as key factors involved in homeostasis maintenance and anti-ageing by Nrf1 via transcriptome sequencing screening. The core essential protein STAG2 (or STAG1), the ATPase subunit SMC3, SMC1, and RAD21, constitute the universally expressed and evolutionary conserved multisubunit protein complex called cohesin, which encircles chromatin [49]. Cohesin exerts a pivotal effect in preserving the structural and functional integrity of genetic material, primarily ensuring sister chromatid cohesion and high-fidelity chromosome separation, facilitating chromosome aggregation, maintaining proper concentration, facilitating error-free DNA damage repair, organizing the genome into large loops, such as topologically associated domains, generating functional domains, and regulating gene expression by integrating transcriptional factors, promoters, enhancers, and RNA polymerase II [50, 51]. Mutations in STAG2, SMC3, and other components of the complex are mutually exclusive (each member serves a distinct function). These mutations (e.g., shortening and frameshift mutations in STAG2 or missense mutations in SMC3) can lead to cohesion dysfunction, resulting in aneuploidy or other abnormalities, ultimately leading to the disruption of cellular homeostasis and triggering cell senescence, apoptosis, neoplasia, etc. [52]. In our study, the deletion of either STAG2 or SMC3 initiated cell senescence in our senescence cell models. We found that Nrf2 deficiency does not affect STAG2 and SMC3 expression; however, different from Nrf2 deficiency, Nrf1 deficiency reduces the expression of STAG2 and SMC3. Subsequent experiments corroborated that Nrf1 specifically modulates the expression of STAG2 and SMC3 by binding to AREs in the STAG2 and SMC3 promoter regions to exert its anti-senescence function through homeostasis maintenance.

Nrf1 and Nrf2 share structural characteristics, similar expression patterns, and identical DNA recognition sites, and they both participate in a myriad of cellular processes together. However, their functions are not entirely analogous, displaying intricate relationships. Reports indicate that, compared to Nrf1 single knockout, Nrf1/Nrf2 double knockout leads to early embryo demise in vivo and elicits elevated levels of intracellular reactive oxygen species in mouse embryonic fibroblast cells in vitro [53, 54], suggesting overlapping biological functions of Nrf1 and Nrf2. Relevant studies have shown that high Nrf1 expression in neurons compensates for Nrf2 deficiency in maintaining cellular redox balance [55]. Moreover, overexpression of either Nrf1 or Nrf2 effectively rescues erastin2-induced ferroptosis in the context of Nrf1 or Nrf2 deficiency [56], revealing an interactive dialogue and

compensatory effects when Nrf1 and Nrf2 overlap in function. Complete excision of Nrf1 in mice gives rise to embryonic lethality, possibly due to enhanced oxidative stress, inadequate erythropoiesis, or insufficient expression of the globin gene [57-59]. In contrast, the knockout of Nrf2 does not result in developmental arrest in mice but increases susceptibility to chemical carcinogens and oxidative stress [60-62]. These studies underscore distinctions in bioactivity between Nrf1 and Nrf2, indicating that there is not complete overlap. Compared to Nrf2, Nrf1 possesses distinct physiological and biological functions that appear to offer greater cellular protection and stress resilience, which are not fully compensated for by Nrf2 or other homologous factors [25]. Primarily, Nrf1 exhibits a multidimensional and layered regulatory landscape. Reportedly, Nrf1 provides greater cardioprotection against ischemic/reperfusion injury in adult mice through a unique dual mechanism involving proteasome activation and redox equilibrium compared to Nrf2 [25]. Our study validates this aspect. In contrast to that of Nrf2, the anti-senescence protection role of Nrf1 relies on multiple mechanisms, encompassing the suppression of the p21-RB stress axis and STAG2/SMC3-induced gene homeostatic balance, autophagy activation, etc. In addition, with regard to equivalent pathways or identical targets, Nrf1 exhibits more robust regulatory effects than Nrf2. Both Nrf1 and Nrf2 can positively regulate PGC1α to maintain mitochondrial integrity and normalize mitochondrial function [46]. However, excessive Nrf2 expression cannot compensate for the absence of PGC1α production due to Nrf1 deficiency. Similarly, our investigation reveals that while both Nrf1 and Nrf2 contribute to anti-senescence by suppressing targets such as p21, the activation of Nrf2 does not inhibit the activation of targets (e.g., p21) following Nrf1 deficiency. Notably, Nrf2 benefits from Keap1 sensors, allowing for a rapid response to external stimuli compared to Nrf1. Nrf1, generally considered a pivotal protective regulator in response to endogenous stress, primarily maintains cellular homeostasis under normal conditions. Our research has revealed notable insights. As is widely established, p21 is a vital downstream target of p53 in senescence [63]. In contrast to senescence observed in *Nrf2*$^{-/-}$ cells, where p53-independent p21 persistent activation occurs, resulting in an increased risk of cell disorders (genomic instability risk, etc.), *Nrf1α*$^{-/-}$ cells exhibit senescence. p21 in *Nrf1α*$^{-/-}$ cells can circumvent the regulatory function of p53. This implies that, compared to Nrf2, Nrf1 exhibits enhanced flexibility in mediating p21 activity to counter senescence. In essence, this revelation underscores the significant and conserved role of Nrf1 in blanacing strength and flexibility in the regulation of key functions, for instance cell fate modulation. This regulatory mechanism achieves both substantive and enduring, as well as precise and efficient control. The essential role of Nrf1 in basal stress response and the maintenance of cellular homeostasis is central to resistance against senescence. Concurrently, Nrf2, operating as a secondary defense mechanism, protects cells against unforeseen exogenous acute stress and is also crucial for anti-senescence. In the context of Nrf1 deficiency, Nrf2 activation serves as a supplemental safeguard mechanism. The multilayered anti-senescence capabilities of organisms depend on the diversity of CNC proteins, which collectively counteract intrinsic and environmental stressors.

In summary, the elusive and complex phenomenon of ageing presents a significant challenge to causal inference due to its intricate relationship with health and disease. The elucidation of the drivers of ageing is crucial for managing associated health risks and disease threats. Cell senescence, a risk factor for organ dysfunction and age-related ailments, plays a key role in unraveling this complexity. Our investigation underscores the critical role of Nrf1, a transcriptional regulator that governs cell function, in counteracting cellular senescence. Nrf1 not only participates in longevity pathways but also serves as an intracellular anti-senescence command center. Given Nrf1's multipolar broad-spectrum regulatory characteristics, our research unveiled various facets of its anti-senescence mechanism. A comprehensive understanding of Nrf1's anti-senescence mechanisms is crucial. Additionally, Nrf1 holds immense promise as a drug target for the prevention and treatment of age-associated disorders and preservation of healthy lifespan. Reportedly, silibinin,

a natural polyphenolic flavonoid from milk thistle seeds, selectively stimulates Nrf1, providing potent cellular protection [64]. Icariin, a promising drug for neurodegenerative disorders, stimulates Nrf1 to elevate Hrd1/synoviolin levels, inhibiting neuroblast apoptosis [65]. ASC-JM17, a new curcumin analogue for the management of spinal and bulbar muscular atrophy, targets Nrf1 for the alleviation of symptoms in this condition [66]. Hence, it is imperative to comprehensively understand Nrf1's anti-senescence mechanisms and fully harness the potency of Nrf1 as a drug target for development. Advancements in Nrf1's anti-senescence realm will significantly contribute to precision health in a rapidly ageing society.

Acknowledgements

We're grateful to all individuals within Zhang's research group for the robust support and assistance throughout the course of this study.

Funding

This research was supported by grants from the National Natural Science Foundation of China(81872336 and 91429305) to Prof. Yiguo Zhang.

Declaration of competing interest

The authors declare that they have no known competing financial interests or personal relationships that could have appeared to influence the work reported in this paper.

Author contributions

Da Lyu designed and executed the experiments, handled the data, produced figures, and prepared Initial manuscript. Conceptualization, Data curation, Formal analysis, Visualization, Writing - original draft. **Meng Wang** contributed to bioinformatics analysis technical assistance. Methodology, Resources. **Lu Qiu** contributed with relevant gene-knockout cell lines design and construction. Methodology, Resources. **Shaofan Hu** contributed to experimental method refinement and technical support. Methodology, Resources. **Yiguo Zhang** supervised all aspects of this study, discussed and helped to analyzed the results, orchestrated all figures, revised and edited this manuscript. Project administration, Conceptualization, Formal analysis, Writing – review & editing, Supervision. This manuscript underwent a thorough review process and received approval from all contributing authors.

Data availability

All necessary data required for assessing the conclusions presented in the paper can be found within the paper itself or in the Supplementary Materials. The additional data supporting this study is available upon reasonable request from the corresponding author.

References

[1] D.J. Panyard, B. Yu, M.P. Snyder, The metabolomics of human aging: Advances, challenges, and opportunities, Science Advances 8(42) (2022) eadd6155.

[2] M.L. Capitano, S.F. Mohamad, S. Cooper, B. Guo, X. Huang, A.M. Gunawan, C. Sampson, J. Ropa, E.F. Srour, C.M. Orschell, Mitigating oxygen stress enhances aged mouse hematopoietic stem cell numbers and function, The Journal of clinical investigation 131(1) (2021).

[3] M.B. Schultz, A.E. Kane, S.J. Mitchell, M.R. MacArthur, E. Warner, D.S. Vogel, J.R. Mitchell, S.E. Howlett, M.S. Bonkowski, D.A. Sinclair, Age and life expectancy clocks based on machine learning analysis of mouse

frailty, Nature communications 11(1) (2020) 4618.
[4] W.H. Organization, Aging and health (2021) https://www. who. int/news-room/fact-sheets/detail/ageing-and-health, Accessed Jan 29 (2022).
[5] B. Lehallier, D. Gate, N. Schaum, T. Nanasi, S.E. Lee, H. Yousef, P. Moran Losada, D. Berdnik, A. Keller, J. Verghese, Undulating changes in human plasma proteome profiles across the lifespan, Nature medicine 25(12) (2019) 1843-1850.
[6] A.J. Scott, M. Ellison, D.A. Sinclair, The economic value of targeting aging, Nature Aging 1(7) (2021) 616-623.
[7] C. López-Otín, M.A. Blasco, L. Partridge, M. Serrano, G. Kroemer, Hallmarks of aging: An expanding universe, Cell (2023).
[8] C. López-Otín, F. Pietrocola, D. Roiz-Valle, L. Galluzzi, G. Kroemer, Meta-hallmarks of aging and cancer, Cell metabolism 35(1) (2023) 12-35.
[9] J. Guo, X. Huang, L. Dou, M. Yan, T. Shen, W. Tang, J. Li, Aging and aging-related diseases: From molecular mechanisms to interventions and treatments, Signal Transduction and Targeted Therapy 7(1) (2022) 391.
[10] R.A. Avelar, J.G. Ortega, R. Tacutu, E.J. Tyler, D. Bennett, P. Binetti, A. Budovsky, K. Chatsirisupachai, E. Johnson, A. Murray, A multidimensional systems biology analysis of cellular senescence in aging and disease, Genome biology 21(1) (2020) 1-22.
[11] N. Zhu, X. Liu, M. Xu, Y. Li, Dietary Nucleotides Retard Oxidative Stress-Induced Senescence of Human Umbilical Vein Endothelial Cells, Nutrients 13(9) (2021) 3279.
[12] T. Tchkonia, A.K. Palmer, J.L. Kirkland, New horizons: novel approaches to enhance healthspan through targeting cellular senescence and related aging mechanisms, The Journal of Clinical Endocrinology & Metabolism 106(3) (2021) e1481-e1487.
[13] A. Hernandez-Segura, J. Nehme, M. Demaria, Hallmarks of cellular senescence, Trends in cell biology 28(6) (2018) 436-453.
[14] M. Xu, T. Pirtskhalava, J.N. Farr, B.M. Weigand, A.K. Palmer, M.M. Weivoda, C.L. Inman, M.B. Ogrodnik, C.M. Hachfeld, D.G. Fraser, Senolytics improve physical function and increase lifespan in old age, Nature medicine 24(8) (2018) 1246-1256.
[15] Y. Cai, H. Zhou, Y. Zhu, Q. Sun, Y. Ji, A. Xue, Y. Wang, W. Chen, X. Yu, L. Wang, Elimination of senescent cells by β-galactosidase-targeted prodrug attenuates inflammation and restores physical function in aged mice, Cell research 30(7) (2020) 574-589.
[16] M. Serrano, D. Munoz-Espin, Cellular Senescence in Disease, Academic Press2021.
[17] S. Song, E.W.-F. Lam, T. Tchkonia, J.L. Kirkland, Y. Sun, Senescent cells: emerging targets for human aging and age-related diseases, Trends in biochemical sciences 45(7) (2020) 578-592.
[18] S.-L. Paiva, Adding to the senolytic arsenal, Nature Reviews Drug Discovery 18(12) (2019) 901-902.
[19] G. Ruvkun, N. Lehrbach, Regulation and functions of the ER-Associated nrf1 transcription factor, Cold Spring Harbor Perspectives in Biology 15(1) (2023) a041266.
[20] H.M. Kim, J.W. Han, J.Y. Chan, Nuclear factor erythroid-2 like 1 (NFE2L1): structure, function and regulation, Gene 584(1) (2016) 17-25.
[21] Y. Zhang, Y. Xiang, Molecular and cellular basis for the unique functioning of Nrf1, an indispensable transcription factor for maintaining cell homoeostasis and organ integrity, Biochemical Journal 473(8) (2016) 961-1000.
[22] K. Yang, R. Huang, H. Fujihira, T. Suzuki, N. Yan, N-glycanase NGLY1 regulates mitochondrial homeostasis and inflammation through NRF1, Journal of Experimental Medicine 215(10) (2018) 2600-2616.

[23] S. Gutbier, A.-S. Spreng, J. Delp, S. Schildknecht, C. Karreman, I. Suciu, T. Brunner, M. Groettrup, M. Leist, Prevention of neuronal apoptosis by astrocytes through thiol-mediated stress response modulation and accelerated recovery from proteotoxic stress, Cell Death & Differentiation 25(12) (2018) 2101-2117.

[24] N.J. Lehrbach, G. Ruvkun, Endoplasmic reticulum-associated SKN-1A/Nrf1 mediates a cytoplasmic unfolded protein response and promotes longevity, Elife 8 (2019) e44425.

[25] M. Cui, A. Atmanli, M.G. Morales, W. Tan, K. Chen, X. Xiao, L. Xu, N. Liu, R. Bassel-Duby, E.N. Olson, Nrf1 promotes heart regeneration and repair by regulating proteostasis and redox balance, Nature communications 12(1) (2021) 5270.

[26] S.R. Nath, Z. Yu, T.A. Gipson, G.B. Marsh, E. Yoshidome, D.M. Robins, S.V. Todi, D.E. Housman, A.P. Lieberman, Androgen receptor polyglutamine expansion drives age-dependent quality control defects and muscle dysfunction, The Journal of Clinical Investigation 128(8) (2018) 3630-3641.

[27] K. Wang, Y. Li, T. Qiang, J. Chen, X. Wang, Role of epigenetic regulation in myocardial ischemia/reperfusion injury, Pharmacological Research 170 (2021) 105743.

[28] M. Wang, Y. Ren, S. Hu, K. Liu, L. Qiu, Y. Zhang, TCF11 Has a Potent Tumor-Repressing Effect Than Its Prototypic Nrf1α by definition of both similar yet different regulatory profiles, with a striking disparity from Nrf2, Frontiers in oncology 11 (2021) 707032.

[29] L. Qiu, M. Wang, S. Hu, X. Ru, Y. Ren, Z. Zhang, S. Yu, Y. Zhang, Oncogenic activation of Nrf2, though as a master antioxidant transcription factor, liberated by specific knockout of the full-length Nrf1α that acts as a dominant tumor repressor, Cancers 10(12) (2018) 520.

[30] B. Langmead, Ultrafast andmemory-efficient alignment of short DNA sequences to the human genome, Genome Biol 10, R25 Genome Biology 10 (2009) R5.

[31] D. Kim, B. Langmead, S.L. Salzberg, HISAT: a fast spliced aligner with low memory requirements, Nature methods 12(4) (2015) 357-360.

[32] B. Li, C.N. Dewey, RSEM: accurate transcript quantification from RNA-Seq data with or without a reference genome, BMC bioinformatics 12 (2011) 1-16.

[33] G.D. Bader, C.W. Hogue, An automated method for finding molecular complexes in large protein interaction networks, BMC bioinformatics 4(1) (2003) 1-27.

[34] C.-H. Chin, S.-H. Chen, H.-H. Wu, C.-W. Ho, M.-T. Ko, C.-Y. Lin, cytoHubba: identifying hub objects and sub-networks from complex interactome, BMC systems biology 8(4) (2014) 1-7.

[35] T. Tchkonia, J.L. Kirkland, Aging, cell senescence, and chronic disease: emerging therapeutic strategies, Jama 320(13) (2018) 1319-1320.

[36] J.M. Van Deursen, The role of senescent cells in ageing, Nature 509(7501) (2014) 439-446.

[37] J. Bi, L. Yang, T. Wang, J. Zhang, T. Li, Y. Ren, M. Wang, X. Chen, Y. Lv, R. Wu, Irisin improves autophagy of aged hepatocytes via increasing telomerase activity in liver injury, Oxidative medicine and cellular longevity 2020 (2020).

[38] V.D. Longo, G.S. Shadel, M. Kaeberlein, B. Kennedy, Replicative and chronological aging in Saccharomyces cerevisiae, Cell metabolism 16(1) (2012) 18-31.

[39] X. Liang, Z. Yan, W. Ma, Y. Qian, X. Zou, Y. Cui, J. Liu, Y. Meng, Peroxiredoxin 4 protects against ovarian ageing by ameliorating D-galactose-induced oxidative damage in mice, Cell Death & Disease 11(12) (2020) 1053.

[40] X. Chu, J. Wen, R.P. Raju, Rapid senescence⌊like response after acute injury, Aging Cell 19(9) (2020) e13201.

[41] A. Kröll⌊Hermi, F. Ebstein, C. Stoetzel, V. Geoffroy, E. Schaefer, S. Scheidecker, S. Bär, M. Takamiya, K. Kawakami, B.A. Zieba, Proteasome subunit PSMC3 variants cause neurosensory syndrome combining

deafness and cataract due to proteotoxic stress, EMBO molecular medicine 12(7) (2020) e11861.
[42] M. Revuelta, A. Matheu, Autophagy in stem cell aging, Aging cell 16(5) (2017) 912-915.
[43] P. Rajendran, A.M. Alzahrani, H.N. Hanieh, S.A. Kumar, R. Ben Ammar, T. Rengarajan, M.A. Alhoot, Autophagy and senescence: A new insight in selected human diseases, Journal of cellular physiology 234(12) (2019) 21485-21492.
[44] I. Dikic, Z. Elazar, Mechanism and medical implications of mammalian autophagy, Nature reviews Molecular cell biology 19(6) (2018) 349-364.
[45] D.C. Rubinsztein, G. Mariño, G. Kroemer, Autophagy and aging, Cell 146(5) (2011) 682-695.
[46] S. Hu, J. Feng, M. Wang, R. Wufuer, K. Liu, Z. Zhang, Y. Zhang, Nrf1 is an indispensable redox-determining factor for mitochondrial homeostasis by integrating multi-hierarchical regulatory networks, Redox Biology 57 (2022) 102470.
[47] L. Gong, D. Cui, D. Liu, X. Shen, H. Pan, X. Xiong, Y. Zhao, FBXW7 inactivation induces cellular senescence via accumulation of p53, Cell Death & Disease 13(9) (2022) 788.
[48] C.L. Xu, B. Sang, G.Z. Liu, J.M. Li, X.D. Zhang, L.X. Liu, R.F. Thorne, M. Wu, SENEBLOC, a long non-coding RNA suppresses senescence via p53-dependent and independent mechanisms, Nucleic acids research 48(6) (2020) 3089-3102.
[49] C. Morales, A. Losada, Establishing and dissolving cohesion during the vertebrate cell cycle, Current opinion in cell biology 52 (2018) 51-57.
[50] J.F. Marko, P. De Los Rios, A. Barducci, S. Gruber, DNA-segment-capture model for loop extrusion by structural maintenance of chromosome (SMC) protein complexes, Nucleic acids research 47(13) (2019) 6956-6972.
[51] C. Meisenberg, S.I. Pinder, S.R. Hopkins, S.K. Wooller, G. Benstead-Hume, F.M. Pearl, P.A. Jeggo, J.A. Downs, Repression of transcription at DNA breaks requires cohesin throughout interphase and prevents genome instability, Molecular cell 73(2) (2019) 212-223. e7.
[52] S. Cuartero, F.D. Weiss, G. Dharmalingam, Y. Guo, E. Ing-Simmons, S. Masella, I. Robles-Rebollo, X. Xiao, Y.-F. Wang, I. Barozzi, Control of inducible gene expression links cohesin to hematopoietic progenitor self-renewal and differentiation, Nature immunology 19(9) (2018) 932-941.
[53] L. Leung, M. Kwong, S. Hou, C. Lee, J.Y. Chan, Deficiency of the Nrf1 and Nrf2 transcription factors results in early embryonic lethality and severe oxidative stress, Journal of Biological Chemistry 278(48) (2003) 48021-48029.
[54] H. Sekine, K. Okazaki, K. Kato, M.M. Alam, H. Shima, F. Katsuoka, T. Tsujita, N. Suzuki, A. Kobayashi, K. Igarashi, O-GlcNAcylation signal mediates proteasome inhibitor resistance in cancer cells by stabilizing NRF1, Molecular and cellular biology 38(17) (2018) e00252-18.
[55] C.S. Lee, C. Lee, T. Hu, J.M. Nguyen, J. Zhang, M.V. Martin, M.P. Vawter, E.J. Huang, J.Y. Chan, Loss of nuclear factor E2-related factor 1 in the brain leads to dysregulation of proteasome gene expression and neurodegeneration, Proceedings of the National Academy of Sciences 108(20) (2011) 8408-8413.
[56] G.C. Forcina, L. Pope, M. Murray, W. Dong, M. Abu-Remaileh, C.R. Bertozzi, S.J. Dixon, Ferroptosis regulation by the NGLY1/NFE2L1 pathway, Proceedings of the National Academy of Sciences 119(11) (2022) e2118646119.
[57] S.C. Farmer, C.-W. Sun, G.E. Winnier, B. Hogan, T.M. Townes, The bZIP transcription factor LCR-F1 is essential for mesoderm formation in mouse development, Genes & development 11(6) (1997) 786-798.
[58] J.Y. Chan, M. Kwong, R. Lu, J. Chang, B. Wang, T.B. Yen, Y.W. Kan, Targeted disruption of the ubiquitous CNC-bZIP transcription factor, Nrf-1, results in anemia and embryonic lethality in mice, The EMBO journal 17(6) (1998) 1779-1787.

[59] L. Chen, M. Kwong, R. Lu, D. Ginzinger, C. Lee, L. Leung, J.Y. Chan, Nrf1 is critical for redox balance and survival of liver cells during development, Molecular and cellular biology 23(13) (2003) 4673-4686.
[60] A. Enomoto, K. Itoh, E. Nagayoshi, J. Haruta, T. Kimura, T. O'Connor, T. Harada, M. Yamamoto, High sensitivity of Nrf2 knockout mice to acetaminophen hepatotoxicity associated with decreased expression of ARE-regulated drug metabolizing enzymes and antioxidant genes, Toxicological Sciences 59(1) (2001) 169-177.
[61] Y. Aoki, H. Sato, N. Nishimura, S. Takahashi, K. Itoh, M. Yamamoto, Accelerated DNA adduct formation in the lung of the Nrf2 knockout mouse exposed to diesel exhaust, Toxicology and applied pharmacology 173(3) (2001) 154-160.
[62] C. Xu, M.-T. Huang, G. Shen, X. Yuan, W. Lin, T.O. Khor, A.H. Conney, A.-N.T. Kong, Inhibition of 7, 12-dimethylbenz (a) anthracene-induced skin tumorigenesis in C57BL/6 mice by sulforaphane is mediated by nuclear factor E2–related factor 2, Cancer research 66(16) (2006) 8293-8296.
[63] T. Nakatsuka, K. Tateishi, H. Kato, H. Fujiwara, K. Yamamoto, Y. Kudo, H. Nakagawa, Y. Tanaka, H. Ijichi, T. Ikenoue, Inhibition of histone methyltransferase G9a attenuates liver cancer initiation by sensitizing DNA-damaged hepatocytes to p53-induced apoptosis, Cell Death & Disease 12(1) (2021) 99.
[64] F. Yang, M. Jia, C. Deng, B. Xiao, R. Dai, Y. Xiang, Silibinin ameliorates cisplatin-induced acute kidney injury via activating nfe2l1-mediated antioxidative response to suppress the ros/mapk signaling pathway, Journal of Molecular Histology 53(4) (2022) 729-740.
[65] F. Li, B. Gao, H. Dong, J. Shi, D. Fang, Icariin induces synoviolin expression through NFE2L1 to protect neurons from ER stress-induced apoptosis, PloS one 10(3) (2015) e0119955.
[66] L.C. Bott, N.M. Badders, K.-I. Chen, G.G. Harmison, E. Bautista, C.C.-Y. Shih, M. Katsuno, G. Sobue, J.P. Taylor, N.P. Dantuma, A small-molecule Nrf1 and Nrf2 activator mitigates polyglutamine toxicity in spinal and bulbar muscular atrophy, Human Molecular Genetics 25(10) (2016) 1979-1989.

Figure Legends

Fig. 1. *Nrf1α*$^{-/-}$ cells acquire several senescent features.

(A and B) SA-β-gal activity in WT and *Nrf1α*$^{-/-}$ cells in our senescence cell models was assessed via staining. (A) Representative images of model 1 and (B) model 2. Scale bars: 50 μm. (C and D) Quantification of SA-β-gal+ cells (positive) in WT and *Nrf1α*$^{-/-}$ cells (C) in model 1 and (D) model 2. Quantitative information is reported as the mean ± SD, based on three individual trials. $$, $p < 0.01$. (E and F) Quantitative analysis of SA-β-gal activity. The enzyme activity is expressed as the generation rate of p-nitrophenol. (E) Comparison of SA-β-gal levels in WT and *Nrf1α*$^{-/-}$ cells between senescence cell model 1 and (F) model 2.Quantitative information is reported as the mean ± SD, based on three individual trials. $, $p < 0.05$; $$, $p < 0.01$. (G and H, left) Colony formation was evaluated for WT and *Nrf1α*$^{-/-}$ cells in the senescence cell models. (G and H, right) The proliferative capacity of WT and *Nrf1α*$^{-/-}$ cells in (G) model 1 and (H) model 2 was measured via the CCK-8 assay. Quantitative information is reported as the mean ± SD, based on three individual trials. **, $p < 0.01$.

Fig. 2. Nrf1-KO induces SASP and the accumulation of senescence biomarkers through the p21 and RB signal transduction pathway.

(A–G) The mRNA expression of SASP-specific markers, namely *IL-1α, IL-1β, IL-6, IL-8, CXCL-3, CXCL-10,* and *MMP1* in WT and *Nrf1α*$^{-/-}$ cells in the senescence cell models, was quantified via RT-qPCR. (A) *IL-1α*; (B) *IL-1β*; (C) *IL-6;* (D) *IL-8*; (E) *CXCL-3*; (F) *CXCL-10*; (G) *MMP1.* Quantitative information is reported as the mean ± SD, based on three individual trials. $$, $p < 0.01$. (H) The distribution of phases in the cell cycle was assessed via flow cytometry. (I) The levels of Ki67, LaminA, p53, p21, CDK2, cyclin D1, pRB, and E2F1 proteins in WT and *Nrf1α*$^{-/-}$ cells in the senescence cell models were analyzed via western blotting. In all immunoblots, intensity was calculated and normalized by β-actin, as shown at the bottom.

Fig. 3. Dysfunctional autophagy contributes to cell senescence in *Nrf1α*$^{-/-}$ cells.

(A–G) The mRNA expression of autophagy-related biomarker molecules, namely *ULK1, Beclin1, ATG4A, ATG7, ATG9A, ATG10,* and *ATG12* in WT and *Nrf1α*$^{-/-}$ cells in the senescence cell models, was quantified via RT-qPCR. (A) *ULK1*; (B) *Beclin1*; (C) A*TG4A*; (D) *ATG7*; (E) *ATG9A*; (F) *ATG10*; (G) *ATG12*. Quantitative information is reported as the mean ± SD, based on three individual trials. *, $p < 0.05$; **, $p < 0.01$. (H) The protein expression of ULK1, Beclin1, ATG5, ATG7, ATG9A, ATG10, ATG13, p62, and LC3 in WT and *Nrf1α*$^{-/-}$ cells in the senescence cell models was assessed via western blotting. In all immunoblots, intensity was calculated and normalized by β-actin, as shown at the bottom. (I) A schematic illustrating the mechanism of Nrf1-deletion induces dysfunctional autophagy.

Fig. 4. Accumulation of Nrf2 exerts a compensatory anti-senescence effect in response to Nrf1 deficiency.

(A) The mean RPKM mRNA values (or fold-change levels) of Nrf1, Nrf2, Keap1, and p62 expressed in HepG2 cells (WT), along with their derivates *Nrf1α*$^{-/-}$, *Nrf2*$^{-/-\Delta TA}$, and *caNrf2*$^{\Delta N}$ cells (29), are shown graphically ,based on three separate tests. *, $p < 0.05$; **, $p < 0.01$; $, $p < 0.05$. (B) The expression of p62, Keap1, Nrf2 proteins in

WT and *Nrf1α*$^{-/-}$ cells in the senescence cell models were assessed via western blotting. In all immunoblots, intensity was calculated and normalized by β-actin, as shown at the bottom. (C) The levels of Nrf2 mRNA in WT and *Nrf1α*$^{-/-}$ cells in the senescence cell models was quantified via RT-qPCR. Quantitative information is reported as the mean ± SD, based on three individual trials. NS = no statistical difference. (D) After transfecting *Nrf1α*$^{-/-}$ HepG2 cells with siNrf2, and the protein level of Nrf2 was assessed via western blotting. In all immunoblots, intensity was calculated and normalized by β-actin, as shown at the bottom. (E–K) The mRNA expression of SASP-specific markers, namely *IL-1α, IL-1β, IL-6, IL-8, CXCL-3, CXCL-10,* and *MMP1,* in *Nrf1α*$^{-/-}$ HepG2 cells with Nrf2 silencing in the senescence cell models was quantified via RT-qPCR. (E) *IL-1α*; (F) *IL-1β*; (G) *IL-6*; (H) *IL-8*; (I) *CXCL-3*; (J) *CXCL-10*; (K) *MMP1*. Quantitative information is reported as the mean ± SD, based on three individual trials. $, $p < 0.05$; $$, $p < 0.01$. (L) After transfecting *Nrf1α*$^{-/-}$ HepG2 cells with siNrf2, The protein levels of Ki67, p53, p21, CDK2, cyclin D1, pRB, and E2F1 were analyzed via western blotting. In all immunoblots, intensity was calculated and normalized by β-actin, as shown at the bottom.

Fig. 5. *Nrf2*$^{-/-}$ cells exhibit several senescent features.

(A) SA-β-gal activity in WT and *Nrf2*$^{-/-}$ cells in our senescence cell models was assessed via staining. Quantitative information is reported as the mean ± SD, based on three individual trials. Scale bars: 50 μm. (B) Quantitative assay of SA-β-gal activity. The enzyme activity is expressed as the generation rate of p-nitrophenol. Quantitative information is reported as the mean ± SD, based on three individual trials. $$, $p < 0.01$. (C–I) The mRNA expression of SASP-specific markers, namely *IL-1α, IL-1β, IL-6, IL-8, CXCL-3, CXCL-10,* and *MMP1,* in WT and *Nrf2*$^{-/-}$ cells in the senescence cell models was quantified via RT-qPCR. (C) *IL-1α*; (D) *IL-1β*; (E) *IL-6*; (F) *IL-8*; (G) *CXCL-3*; (H) *CXCL-10*; (I) *MMP1*. Quantitative information is reported as the mean ± SD, based on three individual trials. $, $p < 0.05$; $$, $p < 0.01$. (J, left) Colony formation was evaluated for WT and *Nrf2*$^{-/-}$ cells in the senescence cell models. (J, right) The proliferative capacity of *WT* and *Nrf2*$^{-/-}$ cells in the senescence cell models was assessed via the CCK-8 assay. Quantitative information is reported as the mean ± SD, based on three individual trials. *, $p < 0.05$. (K–L) The distribution of phases in the cell cycle was assessed via flow cytometry. (K) Distribution of cell cycle phases (%). (L) Flow cytometry histograms. (M) The levels of Ki67, LaminA, p53, p21, CDK2, cyclin D1, pRB, and E2F1 proteins in WT and *Nrf1α*$^{-/-}$ cells in the senescence cell models were analyzed via western blotting. In all immunoblots, intensity was calculated and normalized by β-actin, as shown at the bottom.

Fig. 6. Nrf1, not Nrf2, depends on STAG2 and SMC3 to sustain cellular homeostasis for anti-senescence.

(A) Transcriptome sequencing revealed differentially expressed critical genes regulated by Nrf1 to maintain cellular homeostasis and anti-senescence. A visual representation displaying the expression levels of candidate crucial genes in the form of a heat map. Core target genes (*SMC3* and *STAG2*) are highlighted in blue. (B) The mRNA expression of STAG2 and SMC3 in WT and *Nrf1α*$^{-/-}$ cells was quantified via RT-qPCR. Quantitative information is reported as the mean ± SD, based on three individual trials. *, $p < 0.05$; **, $p < 0.01$. (C and D) The mRNA expression of STAG2 and SMC3 in WT and *Nrf1α*$^{-/-}$ cells in the senescence cell models was quantified via RT-qPCR. mRNA levels of (C) STAG2 and (D) SMC3. Quantitative information is reported as the mean ± SD, based on three individual trials. **, $p < 0.01$. (E and F) the mRNA expression of STAG2 and SMC3 in WT HepG2 cells, *Nrf2*$^{-/-}$ HepG2 cells, *Nrf1α*$^{-/-}$ HepG2 cells, and *Nrf1α*$^{-/-}$ HepG2 cells treated with siNrf2 in the senescence cell models was quantified via RT-qPCR. mRNA levels of (E) STAG2 and (F) SMC3. Quantitative information is reported as the mean ± SD, based on three individual trials. NS = no statistical

difference. (G) The levels of STAG2 and SMC3 proteins in WT cells (HepG2 and LO2 cells), *Nrf1α*$^{-/-}$ cells, WT HepG2 cells, *Nrf2*$^{-/-}$ HepG2 cells, *Nrf1α*$^{-/-}$ HepG2 cells, and *Nrf1α*$^{-/-}$ HepG2 cells exposed to siNrf2 were assessed by western blotting in the senescence cell models. In all immunoblots, intensity was calculated and normalized by β-actin, as shown at the bottom. (I) The potential ARE motifs in the promoters of both the *STAG2* and *SMC3* genes are marked. Three unique ARE-activated reporters and their corresponding mutants were recombined into the pGL3-promoter vector. (i1) *STAG2* gene. (i2) *SMC3* gene. HepG2 cells were transfected with ARE-luc or the corresponding mutant alongside the internal control pRL-TK in conjunction with the Nrf1 expression plasmid or pcDNA3 empty vector. Luciferase activity distinctively driven by AREs was quantified. Quantitative information is reported as the mean ± SD, based on three individual trials. $$, $p < 0.01$; **, $p < 0.01$. (H) Nrf1 ChIP-seq data (in HepG2 cells) was obtained from the Encode platform and analyzed. (h1) Nrf1 engages with the STAG2 promoter regions. (h2) Nrf1 engages with the SMC3 promoter regions.

Fig. 7. STAG2 (or SMC3) deficiency induces cellular senescence.

(A) SA-β-gal activity in STAG2 (or SMC3)-silenced cells in the senescence cell models was assessed via a quantitative assay. (B–H) The mRNA expression of SASP-specific markers, namely *IL-1α, IL-1β, IL-6, IL-8, CXCL-3, CXCL-10*, and *MMP1,* in STAG2 (or SMC3)-silenced cells in the senescence cell models, was quantified via RT-qPCR. (B) *IL-1α*; (C) *IL-1β*; (D) *IL-6*; (E) *IL-8*; (F) *CXCL-3*; (G) *CXCL-10*; (H) *MMP1*. Quantitative information is reported as the mean ± SD, based on three individual trials. $, $p < 0.05$; $$, $p < 0.01$; NS = no statistical difference. (I) The levels of Ki67, LaminA, p53, p21, CDK2, cyclin D1, pRB, and E2F1 proteins in STAG2 (or SMC3)-silenced cells in the senescence cell models were analyzed via western blotting. In all immunoblots, intensity was calculated and normalized by β-actin, as shown at the bottom. (J) A diagram depicting the mechanism by which STAG2 and SMC3 maintain cellular homeostasis and anti-senescence.

Figure 1

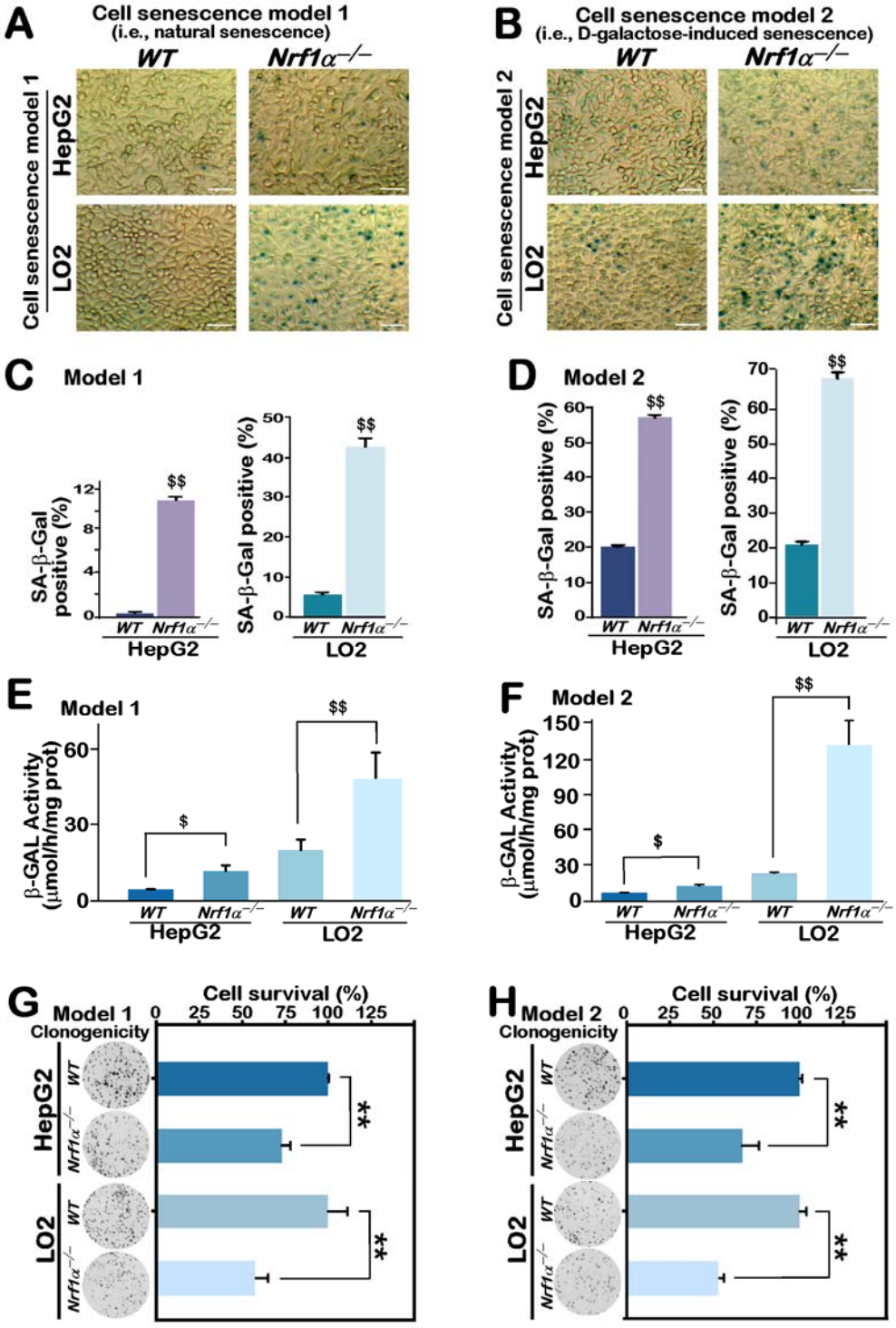
A
Cell senescence model 1
(i.e., natural senescence)
WT
Nrf1α−/−
Cell senescence model 1
HepG2
LO2
B
Cell senescence model 2
(i.e., D-galactose-induced senescence)
WT
Nrf1α−/−
Cell senescence model 2
HepG2
LO2
C
Model 1
SA-β-Gal positive (%)
$$
WT
Nrf1α−/−
HepG2
LO2
D
Model 2
SA-β-Gal positive (%)
$$
WT
Nrf1α−/−
HepG2
LO2
E
Model 1
β-GAL Activity (μmol/h/mg prot)
$
$$
WT
Nrf1α−/−
HepG2
LO2
F
Model 2
β-GAL Activity (μmol/h/mg prot)
$
$$
WT
Nrf1α−/−
HepG2
LO2
G
Model 1
Clonogenicity
Cell survival (%)
HepG2
LO2
WT
Nrf1α−/−
**
H
Model 2
Clonogenicity
Cell survival (%)
HepG2
LO2
WT
Nrf1α−/−
**

Figure 2

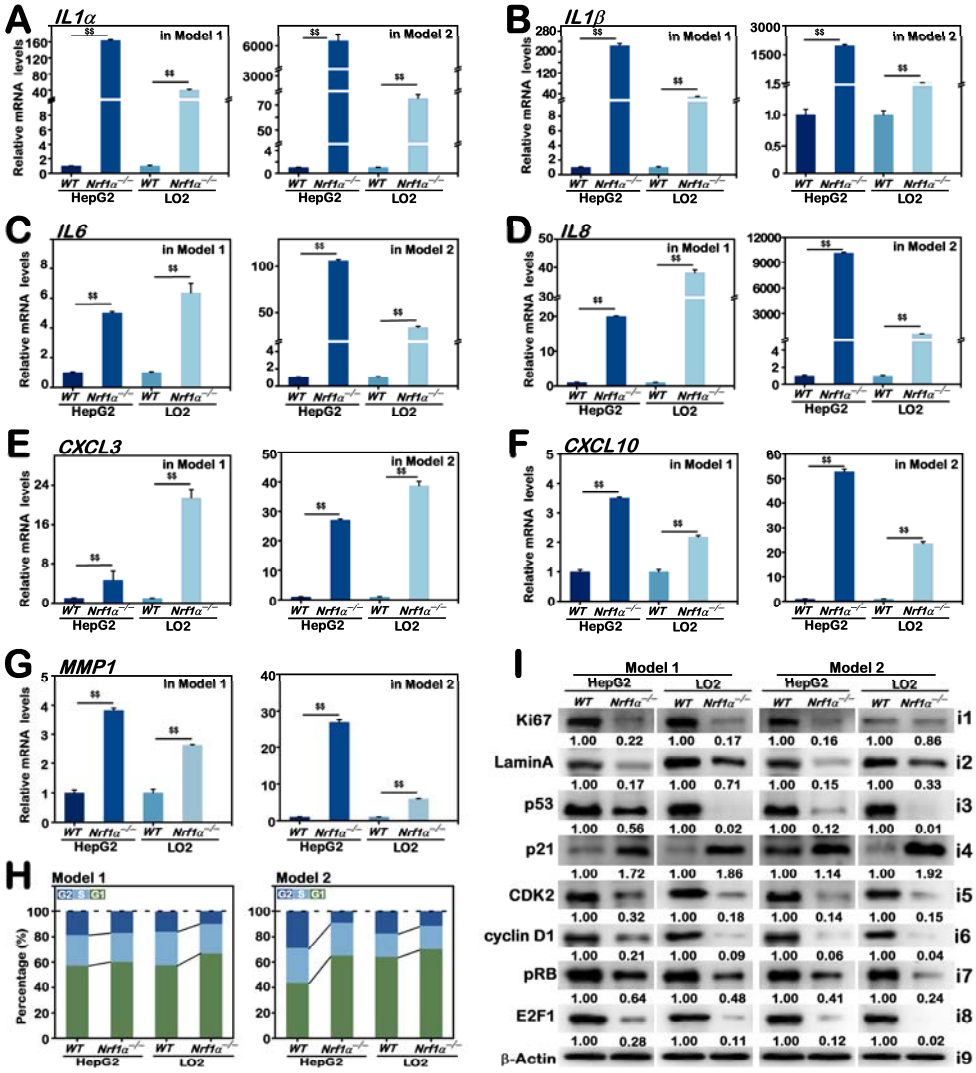
A
IL1α
in Model 1
in Model 2
B
IL1β
C
IL6
D
IL8
E
CXCL3
F
CXCL10
G
MMP1
Relative mRNA levels
WT
Nrf1α−/−
HepG2
LO2
H
Model 1
Model 2
Percentage (%)
G2
S
G1
I
Model 1
Model 2
Ki67
LaminA
p53
p21
CDK2
cyclin D1
pRB
E2F1
β-Actin
i1
i2
i3
i4
i5
i6
i7
i8
i9

Figure 3

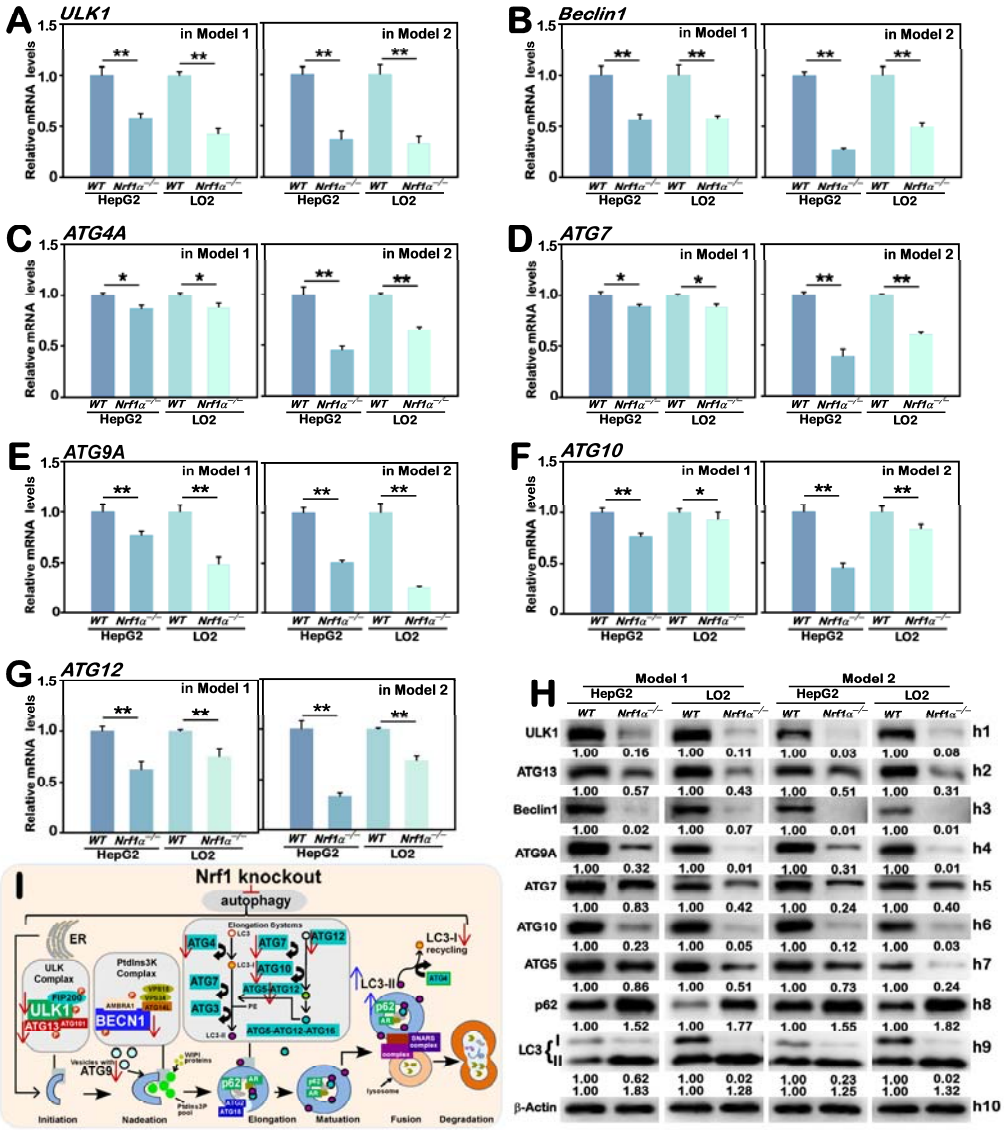
A ULK1
B Beclin1
C ATG4A
D ATG7
E ATG9A
F ATG10
G ATG12
in Model 1
in Model 2
Relative mRNA levels
WT
Nrf1α−/−
HepG2
LO2
H
Model 1
Model 2
ULK1
ATG13
Beclin1
ATG9A
ATG7
ATG10
ATG5
p62
LC3
β-Actin
h1
h2
h3
h4
h5
h6
h7
h8
h9
h10
I
Nrf1 knockout
autophagy
ER
ULK Complex
PtdIns3K Complex
BECN1
Elongation Systems
LC3-I recycling
LC3-II
ATG5-ATG12-ATG16
Initiation
Nadeation
Elongation
Matuation
Fusion
Degradation

Figure 4

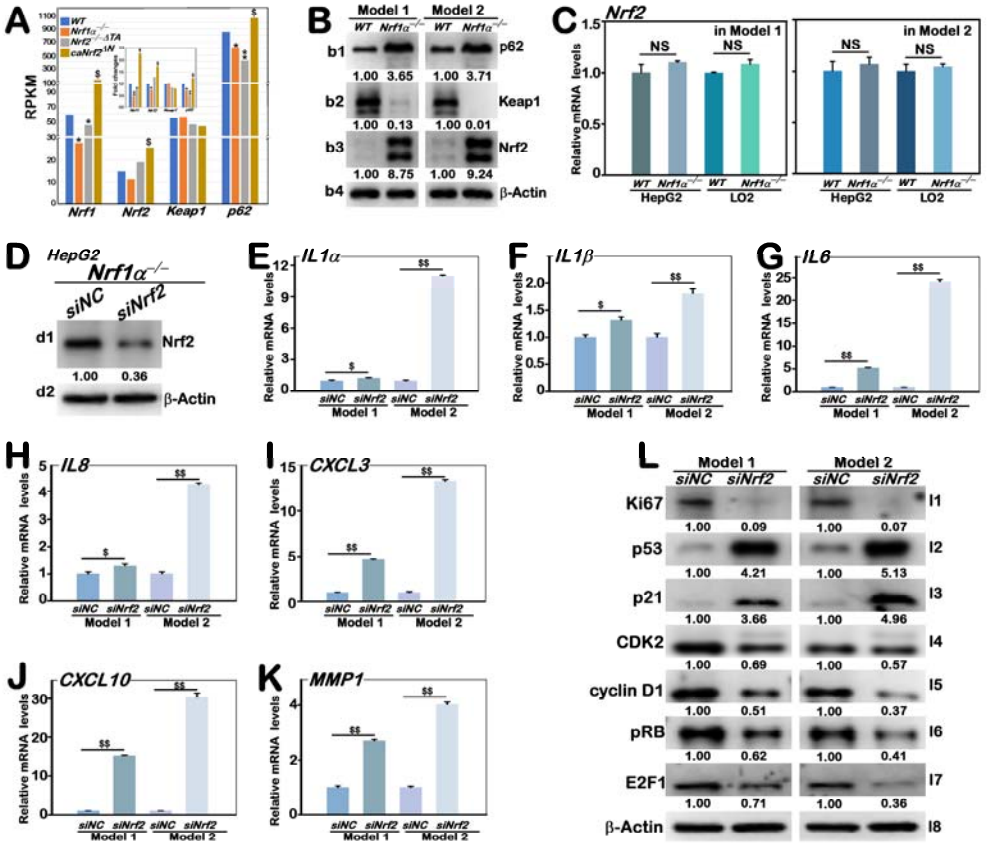
A
RPKM
Nrf1
Nrf2
Keap1
p62
B
Model 1
Model 2
WT
Nrf1α-/-
b1
b2
b3
b4
p62
Keap1
Nrf2
β-Actin
1.00 3.65
1.00 3.71
1.00 0.13
1.00 0.01
1.00 8.75
1.00 9.24
C
Nrf2
in Model 1
in Model 2
NS
Relative mRNA levels
HepG2
LO2
D
HepG2
Nrf1α-/-
siNC
siNrf2
d1
d2
Nrf2
β-Actin
1.00 0.36
E
IL1α
F
IL1β
G
IL6
H
IL8
I
CXCL3
J
CXCL10
K
MMP1
Relative mRNA levels
Model 1
Model 2
L
Ki67
p53
p21
CDK2
cyclin D1
pRB
E2F1
β-Actin
1.00 0.09
1.00 0.07
1.00 4.21
1.00 5.13
1.00 3.66
1.00 4.96
1.00 0.69
1.00 0.57
1.00 0.51
1.00 0.37
1.00 0.62
1.00 0.41
1.00 0.71
1.00 0.36
I1
I2
I3
I4
I5
I6
I7
I8

Figure 5

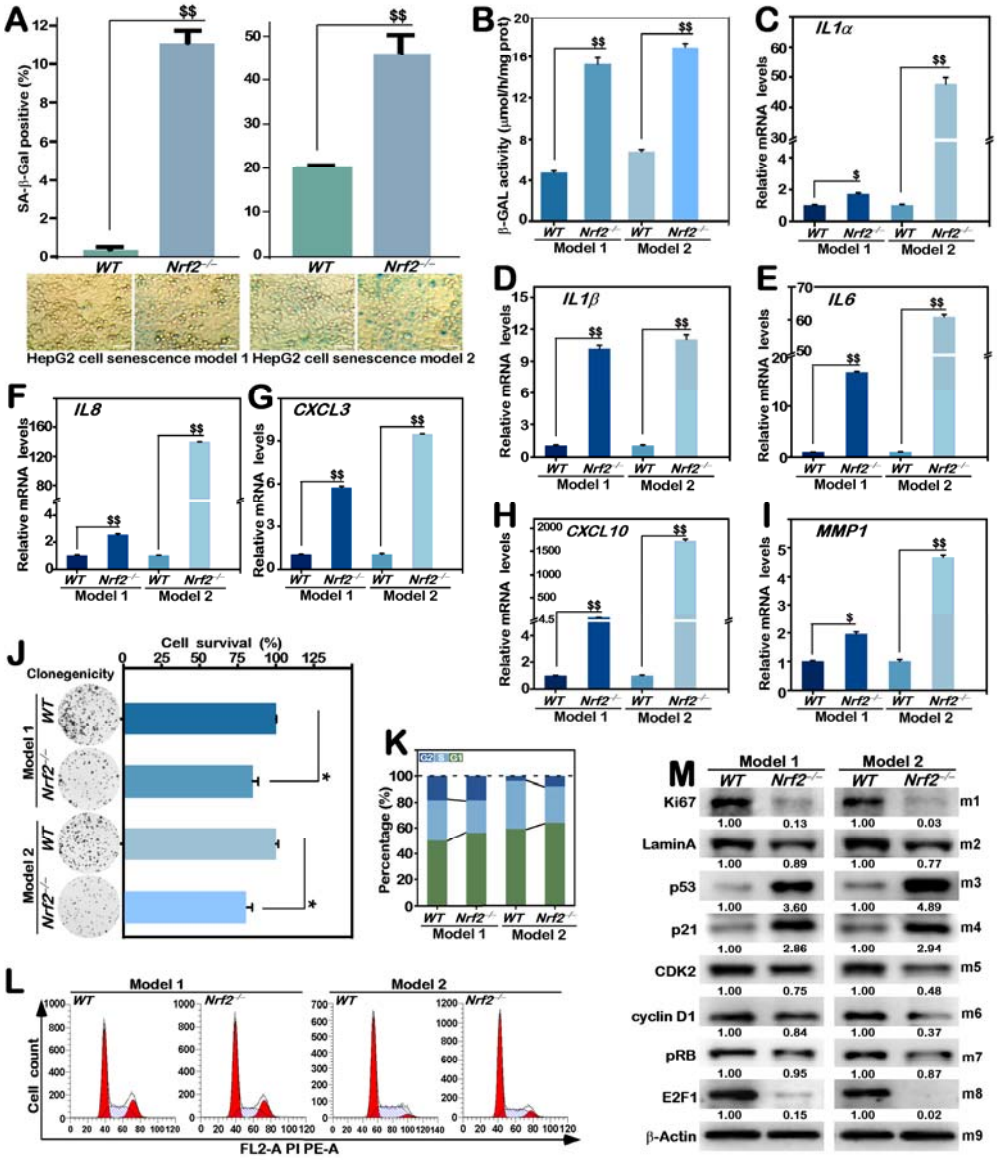
A
SA-β-Gal positive (%)
WT
Nrf2-/-
HepG2 cell senescence model 1
HepG2 cell senescence model 2
B
β-GAL activity (μmol/h/mg prot)
Model 1
Model 2
C
IL1α
Relative mRNA levels
D
IL1β
E
IL6
F
IL8
G
CXCL3
H
CXCL10
I
MMP1
J
Cell survival (%)
Clonegenicity
K
Percentage (%)
L
Cell count
FL2-A PI PE-A
M
Ki67
LaminA
p53
p21
CDK2
cyclin D1
pRB
E2F1
β-Actin
m1
m2
m3
m4
m5
m6
m7
m8
m9

Figure 6

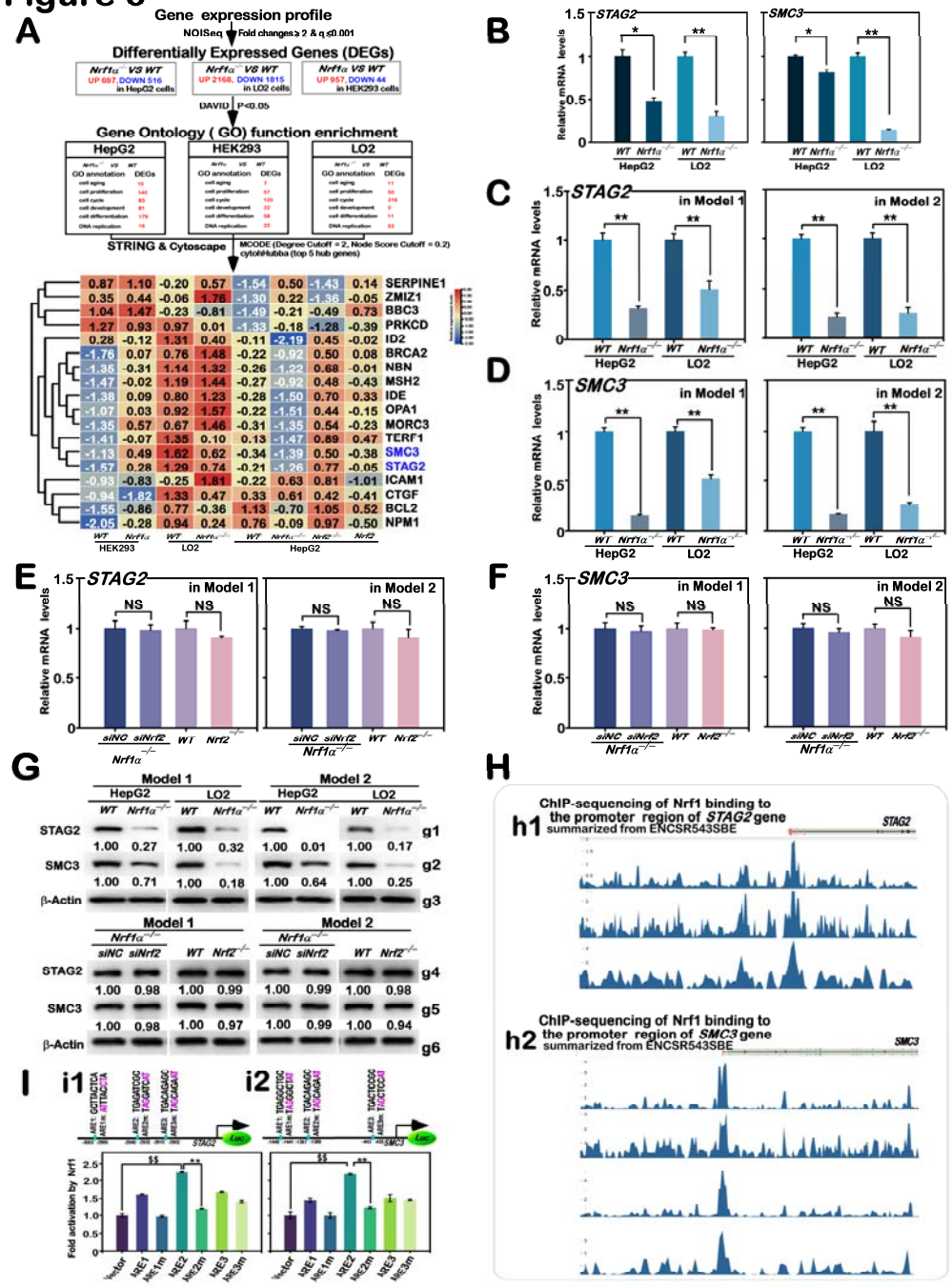

A
Gene expression profile
NOISeq Fold changes ≥ 2 & q ≤0.001
Differentially Expressed Genes (DEGs)
Nrf1α⁻/⁻ VS WT
UP 697, DOWN 516
in HepG2 cells
Nrf1α⁻/⁻ VS WT
UP 2168, DOWN 1815
in LO2 cells
Nrf1α VS WT
UP 957, DOWN 44
in HEK293 cells
DAVID P<0.05
Gene Ontology (GO) function enrichment
HepG2
HEK293
LO2
STRING & Cytoscape
MCODE (Degree Cutoff = 2, Node Score Cutoff = 0.2)
cytohHubba (top 5 hub genes)
SERPINE1
ZMIZ1
BBC3
PRKCD
ID2
BRCA2
NBN
MSH2
IDE
OPA1
MORC3
TERF1
SMC3
STAG2
ICAM1
CTGF
BCL2
NPM1
B
STAG2
SMC3
Relative mRNA levels
C
in Model 1
in Model 2
D
E
F
NS
G
Model 1
Model 2
STAG2
SMC3
β-Actin
g1
g2
g3
g4
g5
g6
H
h1
ChIP-sequencing of Nrf1 binding to the promoter region of STAG2 gene
summarized from ENCSR543SBE
h2
ChIP-sequencing of Nrf1 binding to the promoter region of SMC3 gene
summarized from ENCSR543SBE
I
i1
i2
Fold activation by Nrf1
Vector
MRE1
MRE1m
MRE2
MRE2m
MRE3
MRE3m

Figure7

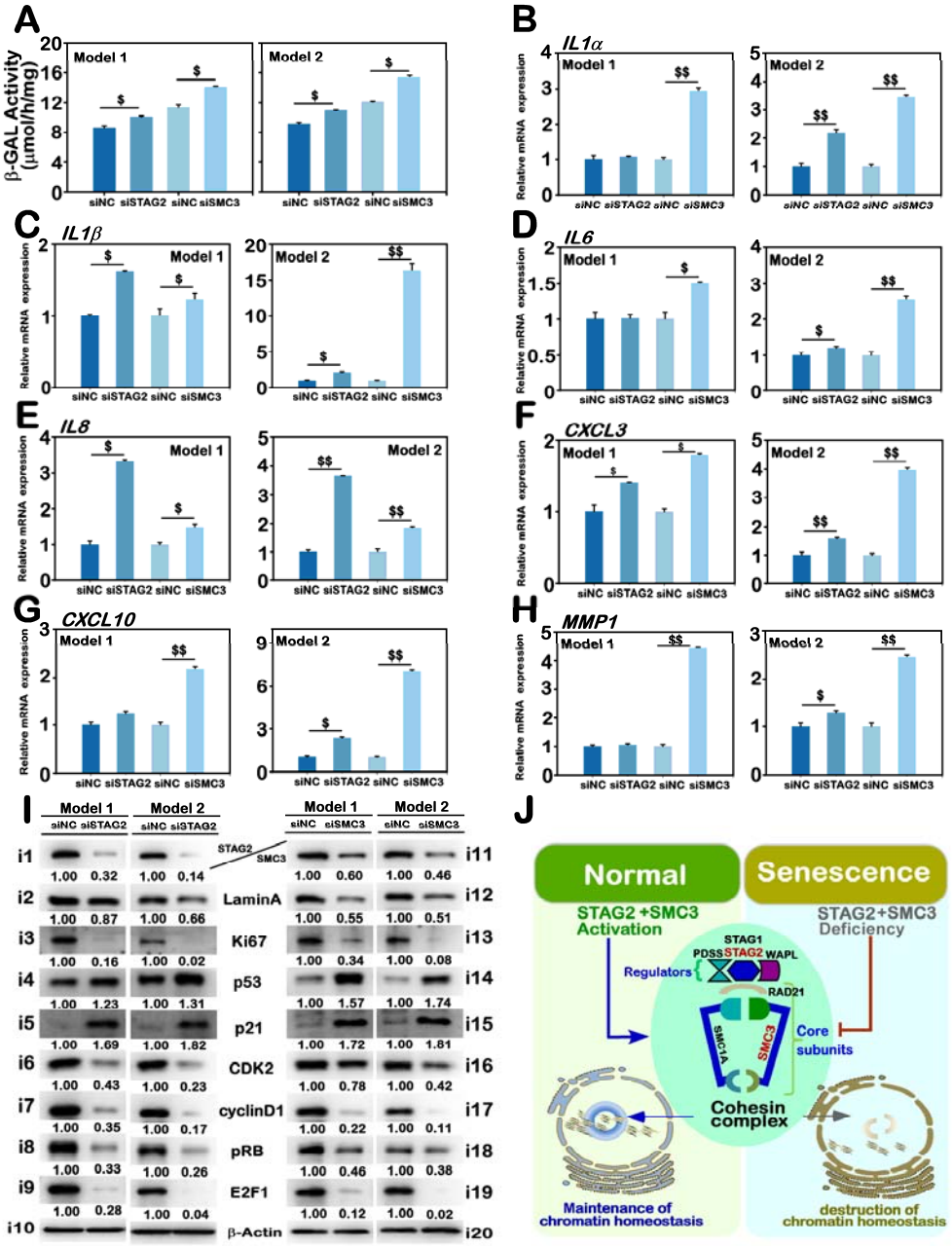
A
β-GAL Activity (μmol/h/mg)
Model 1
Model 2
siNC siSTAG2 siNC siSMC3
B
IL1α
Relative mRNA expression
C
IL1β
D
IL6
E
IL8
F
CXCL3
G
CXCL10
H
MMP1
I
Model 1
Model 2
siNC siSTAG2
siNC siSMC3
STAG2
SMC3
LaminA
Ki67
p53
p21
CDK2
cyclinD1
pRB
E2F1
β-Actin
J
Normal
Senescence
STAG2 +SMC3 Activation
STAG2+SMC3 Deficiency
Regulators
STAG1
PDSS
STAG2
WAPL
RAD21
SMC1A
SMC3
Core subunits
Cohesin complex
Maintenance of chromatin homeostasis
destruction of chromatin homeostasis